
Article:
Ilin, Konstantin and Morgulis, Andrey (2022) The effect of boundary conditions on the stability of two-dimensional flows in an annulus with permeable boundary. Physics of fluids. 074117. ISSN: 1070-6631

https://doi.org/10.1063/5.0100090

Physics of Fluids

The effect of boundary conditions on the stability of two-dimensional flows in an annulus with permeable boundary

Cite as: Phys. Fluids **34**, 074117 (2022); https://doi.org/10.1063/5.0100090
Submitted: 20 May 2022 • Accepted: 02 July 2022 • Accepted Manuscript Online: 05 July 2022 • Published Online: 22 July 2022

Published open access through an agreement with JISC Collections

K. Ilin and A. Morgulis

Physics of Fluids ARTICLE scitation.org/journal/phf

The effect of boundary conditions on the stability of two-dimensional flows in an annulus with permeable boundary

Cite as: Phys. Fluids **34**, 074117 (2022); doi: 10.1063/5.0100090
Submitted: 20 May 2022 · Accepted: 2 July 2022 ·
Published Online: 22 July 2022

K. Ilin[1,a)] and A. Morgulis[2]

AFFILIATIONS

[1]Department of Mathematics, University of York, Heslington, York YO10 5DD, United Kingdom
[2]Vorovich Institute of Mathematics, Mechanics and Computer Science, The Southern Federal University, Rostov-on-Don, and The Southern Mathematical Insitutute, VSC Scientific Center RAS, Vladikavkaz, Russian Federation

[a)]Author to whom correspondence should be addressed: konstantin.ilin@york.ac.uk

ABSTRACT

Our aim is to study the effect of the outflow boundary conditions on the stability of incompressible flows in a domain with a permeable boundary. For this purpose, we examine the stability of the Couette flow with the radial throughflow between permeable cylinders. Most earlier studies of this flow employed the boundary conditions that prescribe all components of the flow velocity on both cylinders. Taking these boundary conditions as a reference point, we investigate the effect of imposing different outflow boundary conditions. These conditions prescribe the normal stress and either the tangential velocity or the tangential stress. It turns out that both sets of boundary conditions make the corresponding steady flows more unstable. In particular, it is shown that even the classical (purely azimuthal) Couette flow becomes unstable to two-dimensional perturbations if one of the cylinders is permeable and the normal stress (rather than normal velocity) is prescribed on that cylinder.

I. INTRODUCTION

In this paper, we study the stability of the Couette flow with radial throughflow between two permeable circular cylinders. The stability of steady flows of this type has been studied by many authors (see Refs. 1–15). Most papers were motivated by applications to dynamic filtration devices (see, e.g., Refs. 16 and 17) and vortex flow reactors (see Ref. 18 and references therein). It was also argued in Refs. 8 and 10 that such flows may have some relevance to astrophysical flows in accretion disks (see also Ref. 19). Similar inviscid flows have been also used as a model of a flow in the vaneless diffuser of a radial pump.[20–22]

In all these papers (except the ones on the flow in vaneless diffusers), all components of the velocity vector are prescribed on the permeable boundary of the flow domain. In what follows, these boundary conditions are called the reference boundary conditions. They are commonly used for modeling flows with injection/suction of the fluid through porous walls. This approach ignores the problem of modeling the flow in the porous medium and effectively assumes that it is known. However, real flows involve a multitude of physically different permeable boundaries for which very different boundary conditions may turn out to be suitable. At the same time, it is known that a change in the boundary conditions at the inflow and/or outflow boundaries can have a considerable effect on the stability properties of the flow. This is so, for example, for a simple swirling flow in a pipe of finite length.[23] It is, therefore, natural to raise the same question for other simple flows. In the present paper, we study the effect of changing the outflow boundary conditions on the stability of the Couette flow with radial throughflow between rotating permeable cylinders.

We focus on the following boundary conditions, different from the reference conditions. At the inflow part of the boundary (the flow inlet), which is either the inner or the outer cylinder, we specify all components of the velocity. At the outflow part (the flow outlet), represented by the other cylinder, the viscous normal stress in the free fluid is balanced by a given pressure and, in addition to that, either the tangential stress or the tangential velocity is prescribed. Since the normal stress contains the pressure, these two sets of boundary conditions

will be referred to as the pressure–stress and pressure-no-slip conditions. Both sets of conditions arise in weak formulations of the Navier–Stokes equations (see, e.g., Refs. 24 and 25). The relevance of these boundary conditions to real flows will be discussed in Sec. II B.

For both types of conditions at the outlet, the corresponding boundary-value problems formally reduce to the same inviscid problem for the Euler equations in the limit of high radial Reynolds numbers (based on the radial velocity at the inner cylinder and its radius). In the inviscid problem, the boundary conditions at the inlet remain the same (as those in the viscous problem), while only the pressure is prescribed at the outlet. This suggests that in both viscous problems, an inviscid instability, similar to that studied earlier,[10,12] is likely to occur for sufficiently high radial Reynolds numbers.

In the case of the reference conditions, it had been shown[10,12,13] that for sufficiently high radial Reynolds numbers, the basic steady flow between rotating permeable cylinders becomes unstable to two-dimensional (axially independent) azimuthal waves and that the mechanism of the instability is inviscid. Studies of the three-dimensional problem[14,15] had shown that this instability becomes dominant in a wide range of parameters of the problem and, in particular, at rather moderate values of the radial Reynolds number. Thus, the two-dimensional problem has proved useful in studying the stability of the Couette flow with radial throughflow. Since the dependence of the inviscid instability on flow details at the outlet is weak,[10,12] it is natural to expect that two-dimensional inviscid instability will also occur in the case of different boundary conditions at the outlet, so that the two-dimensional stability problem remains relevant to the stability of real Couette flows with radial throughflow. Given that the two dimensional stability problem is computationally much easier and the results are likely to be useful in the three-dimensional problem, we restrict our study to the two-dimensional case. An example of solving the three-dimensional inviscid stability problem that supports the above argument will be presented in Sec. III.

For both types of viscous boundary conditions, we investigate the linear stability of the Couette flow with radial throughflow. Numerical calculations show that for high radial Reynolds numbers, the stability properties of the viscous flows are well described by the inviscid theory, while for small and moderate values of the radial Reynolds number, the stability properties for both types of the outlet boundary conditions may be very different from what was found in Ref. 13 for the reference problem. In particular, in the problem with the pressure-no-slip conditions, it turns out that the corresponding Couette flow is unstable at arbitrarily small radial Reynolds numbers. In this case, it is possible to construct an asymptotic approximation of the linear stability problem, which agrees with numerical results. An interesting by-product of this asymptotic approximation is that a particular case of the classical Couette flow (with purely azimuthal velocity), where one cylinder is impermeable and rotating and the other one is permeable and stationary, turns out to be unstable to two-dimensional perturbations provided the normal stress condition (instead of the normal velocity condition) at the permeable cylinder is imposed. This is strikingly different from the classical Couette flow, which is stable to two-dimensional perturbations. Another unexpected result, valid for both types of boundary conditions, is that there are flow regimes where the converging flows are unstable even if the azimuthal velocity at the inlet is zero.

This paper is organized as follows: Sec. II contains a formulation of the problem, including a discussion of the physical relevance of the boundary conditions. Inviscid stability results are briefly described in Sec. III. Results of numerical solution of the viscous stability problem are presented in Sec. IV. Section V contains a discussion of the results.

II. FORMULATION OF THE PROBLEM

A. Governing equations

We consider two-dimensional (axially independent) viscous incompressible flows in a gap between two concentric cylinders with radii r_1 and r_2 ($r_2 > r_1$). The cylinders are permeable for the fluid, and there is a constant volume flux $2\pi Q$ (per unit length along the common axis of the cylinders) of the fluid through the gap. We shall call the flow diverging if the fluid is pumped into the gap at the inner cylinder and taken out at the outer one and converging if the flow direction is reversed (i.e., the fluid enters the gap at the outer cylinder and leaves it at the inner one). The quantity Q is positive for the diverging flow and negative for the converging flow. For later use, we define the parameter

$$\beta = \frac{Q}{|Q|},$$

so that $\beta = 1$ for the diverging flow and $\beta = -1$ for the converging flow.

Suppose that r_1 is taken as a length scale, $r_1^2/|Q|$ as a timescale, $|Q|/r_1$ as a scale for the velocity, and $\rho Q^2/r_1^2$ for the pressure where ρ is the fluid density. Then, the two-dimensional Navier–Stokes equations, written in non-dimensional variables, have the following form:

$$u_t + uu_r + \frac{v}{r}u_\theta - \frac{v^2}{r} = -p_r + \frac{1}{R}\left(\nabla^2 u - \frac{u}{r^2} - \frac{2}{r^2}v_\theta\right), \quad (1)$$

$$v_t + uv_r + \frac{v}{r}v_\theta + \frac{uv}{r} = -\frac{1}{r}p_\theta + \frac{1}{R}\left(\nabla^2 v - \frac{v}{r^2} + \frac{2}{r^2}u_\theta\right), \quad (2)$$

$$\frac{1}{r}(ru)_r + \frac{1}{r}v_\theta = 0, \quad (3)$$

where (r, θ) are the polar coordinates, u and v are the radial and azimuthal components of the velocity, p is the pressure, $R = |Q|/\nu$ is the radial Reynolds number (ν is the kinematic viscosity of the fluid), and ∇^2 is the polar form of the Laplace operator,

$$\nabla^2 = \partial_r^2 + \frac{1}{r}\partial_r + \frac{1}{r^2}\partial_\theta^2.$$

Both components of the velocity are prescribed at the inlet

$$u|_{r=1} = 1, \quad v|_{r=1} = \gamma_1 \quad (4)$$

for the diverging flow ($\beta = 1$) and

$$u|_{r=a} = -\frac{1}{a}, \quad v|_{r=a} = \frac{\gamma_2}{a} \quad (5)$$

for the converging flow ($\beta = -1$). Here, $a = r_2/r_1$ and $\gamma_{1,2}$ are constants ($\gamma_{1,2}$ are the ratios of the azimuthal velocity to the radial velocity at the inner and outer cylinders, respectively).

If both components of the velocity were also prescribed at the outlet, we would get the reference problem studied previously. Instead, we consider two sets of alternative conditions at the outlet.

(i) The pressure–stress conditions: for the diverging flows, these are given by

$$\left(-p+\frac{2}{R}u_r\right)\Big|_{r=a}=-p_0, \tag{6}$$

$$\frac{1}{R}\left(\frac{1}{r}u_\theta+v_r-\frac{1}{r}v\right)\Big|_{r=a}=s_0, \tag{7}$$

and, for the converging flows, by

$$\left(-p+\frac{2}{R}u_r\right)\Big|_{r=1}=-p_0, \tag{8}$$

$$\frac{1}{R}\left(\frac{1}{r}u_\theta+v_r-\frac{1}{r}v\right)\Big|_{r=1}=s_0, \tag{9}$$

where p_0 and s_0 are constants. Here, p_0 is the dimensionless pressure at the outlet and, for the diverging flows, s_0 is the (dimensionless) external tangential force per unit area. For the converging flow, the sign of s_0 in Eq. (9) is chosen so as to make this condition look similar to condition (7). This means that $(-s_0)$ [not s_0 as in Eq. (7)] is the external tangential force (per unit area).

(ii) The pressure-no-slip conditions are

$$\left(-p+\frac{2}{R}u_r\right)\Big|_{r=a}=-p_0, \quad v|_{r=a}=\frac{\gamma_2}{a} \tag{10}$$

for the diverging flow and

$$\left(-p+\frac{2}{R}u_r\right)\Big|_{r=1}=-p_0, \quad v|_{r=1}=\gamma_1 \tag{11}$$

for the converging flow.

B. On relevance of the pressure-no-slip and pressure–stress conditions to real flows

1. The pressure-no-slip conditions

There are numerous papers on boundary conditions on an interface between a free fluid and a porous medium (see, e.g., Refs. 26–28). There seems to be a consensus that the normal velocity and the normal stress must be continuous across the interface. As for the tangential velocity, either the no-slip condition (with the tangential velocity in the porous medium being zero) or the Beavers–Joseph or Saffman conditions[26,27] are used. In what follows, we assume that the permeability of the porous medium in the tangential direction is much smaller than its permeability in the normal direction, so that the tangential velocity in the walls is very small and can be ignored. As a result, we have the no-slip condition for the free fluid velocity. There are still two more conditions on the interface (for the normal velocity and the normal stress). If we want to decouple the flow of the free fluid from the flow in the porous medium and assume that the latter is known, one of these conditions should be discarded in order to obtain a solvable problem for the Navier–Stokes equations. The most common approach[1,2,6–11,13,15] is to assume that the normal velocity in the porous medium is known and discard the condition for the normal stress. The result will be the reference boundary conditions. Sometimes, however, it is necessary to keep the condition for normal stress because it is preferable to assume that the pressure (rather than the normal velocity) in the porous medium is known or simply because it would be too restrictive to prescribe the normal velocity. Indeed, suppose that we study the stability of purely azimuthal flow between rotating porous cylinders to initial perturbations that do not change the boundary data. Then, if we use the reference boundary conditions, the perturbation velocity will have to be zero at both cylinders and we end up with the stability problem for the classical Couette flow between rotating impermeable cylinders, so that the fact that the cylinders are porous does not make any difference. However, if we prescribe the normal stress instead of the normal velocity, there will be perturbations with the nonzero normal velocity at the porous cylinders, and this wider class of perturbations looks more reasonable physically.

Here is a concrete example of a flow where the pressure-no-slip conditions may be appropriate. Consider a flow between rotating permeable cylinders and suppose that the cylinder representing the outlet is a thin highly permeable membrane, whose permeability is due to many, evenly (or randomly) spaced holes, with a considerable fraction of the holes per unit area of the membrane. If the thickness of the membrane is sufficiently small (smaller than the averaged diameter of the holes), we can ignore the pressure difference across the membrane and assume that the pressure in the membrane on the free fluid–membrane interface is the same as the given pressure on the other side of the membrane. The total normal force applied to a fluid element on the interface must be zero (otherwise it will experience infinite acceleration). As a result, we have the boundary condition that the normal stress at the interface is given by the known pressure on the other side of the membrane. Furthermore, since the tangential permeability of the membrane is zero, the flow through each hole can be assumed to be nearly radial, so that, at first approximation, the no-slip condition for the tangential velocity can be imposed.

The pressure–stress conditions are widely used in modeling open flows where only a part of the flow is studied, and the domain of interest is bounded, entirely or partially, by an artificial boundary. Consider, for example, an open flow through a finite domain where the velocity at the inlet (but not at the outlet) is known and the fluid exits the domain of interest to a very large reservoir containing the same fluid. If we ignore the pressure changes throughout the reservoir and assume that it is almost constant, then it is natural to impose the condition that the normal force acting on the fluid at the outlet is a force due to the pressure outside. Of course, this is not the only possible condition and other conditions may be chosen [e.g., one can simply impose the pressure at the outlet (e.g., Ref. 21) or the condition that the normal derivative of the normal velocity is zero (e.g., Refs. 24 and 29)]. The second boundary condition that is most widely used is that the tangential force exerted on the fluid at the outlet is zero. Although it is not the only possible choice of the second condition (see, e.g., Ref. 24), this condition (or a similar, so-called "do-nothing" condition) is employed in numerous works to model different flows ranging from flows past an obstacle[30,31] to blood flows in arteries.[32,33] In the present paper, we focus on the case where the tangential stress at the outlet is zero [i.e., $s_0=0$ in Eqs. (7) and (9)] because it is this condition that often appears in the literature. The results below may shed some light onto the upstream influence of this condition.

C. Basic flow

Steady rotationally symmetric flows whose stability we want to examine are given by

$$u = \frac{\beta}{r}, \quad v = V(r) = A\, r^{\beta R+1} + \frac{B}{r}, \tag{12}$$

where constants A and B are different for different boundary conditions at the outlet. For both sets of boundary conditions, the pressure is given by

$$p = P(r) = p_0 - \frac{2R^{-1}}{a^2} - \frac{1}{2}\left(\frac{1}{r^2} - \frac{1}{a^2}\right) - \int_r^a \frac{V^2(s)}{s}\, ds$$

for the diverging flow ($\beta = 1$) and

$$p = P(r) = p_0 + 2R^{-1} + \frac{1}{2}\left(1 - \frac{1}{r^2}\right) + \int_1^r \frac{V^2(s)}{s}\, ds$$

for the converging flow ($\beta = -1$).

1. The pressure-stress conditions

Constants A and B are given by the following formulas:

$$A = \frac{(s_0 + 2\gamma_1 a^{-2} R^{-1}) a^{-R}}{1 + 2R^{-1} a^{-(2+R)}}, \quad B = \frac{\gamma_1 - s_0 a^{-R}}{1 + 2R^{-1} a^{-(2+R)}} \tag{13}$$

for the diverging flow ($\beta = 1$) and

$$A = -\frac{s_0 + 2\gamma_2 R^{-1}}{1 - 2R^{-1} a^{2-R}}, \quad B = \frac{\gamma_2 + s_0 a^{2-R}}{1 - 2R^{-1} a^{2-R}} \tag{14}$$

for the converging flow ($\beta = -1$). Note that constants A and B, given by Eq. (13), are well-defined for all $R > 0$, while Eq. (14) defines A and B for all positive R except $R = 2$ (because the denominator in the expressions for A and B vanishes). In the particular case of $\beta = -1$ and $R = 2$, the solution is given by

$$u = -\frac{1}{r}, \quad v = V(r) = \tilde{A}\, \frac{\ln r}{r} + \frac{\tilde{B}}{r}, \tag{15}$$

where

$$\tilde{A} = \frac{2\gamma_2 + s_0}{1 + 2\ln a}, \quad \tilde{B} = \frac{\gamma_2 - 2s_0 \ln a}{1 + 2\ln a}.$$

The dependence of the steady flow (12)–(14) on R is non-trivial, and, for $R \gg 1$, it has a boundary layer either at the outer cylinder (for the diverging flow) or at the inner one (for the converging flow).

It can be shown that, for $R \gg 1$, the azimuthal velocity profile is well approximated by the following asymptotic formula:

$$V(r) = \begin{cases} \gamma_1/r + s_0 a\, e^{-\eta} + O(R^{-1}) & \text{for } \beta = 1, \\ \gamma_2/r - s_0\, e^{-\xi} + O(R^{-1}) & \text{for } \beta = -1, \end{cases} \tag{16}$$

where $\xi = R(r-1)$ and $\eta = R(1 - r/a)$. Note that if $s_0 = 0$ (or if $s_0 \lesssim R^{-1}$ as $R \to \infty$), the above asymptotic formula is different,

$$V(r) = \begin{cases} \gamma_1/r + \dfrac{2\gamma_1}{a}\, e^{-\eta} R^{-1} + O(R^{-2}) & \text{for } \beta = 1, \\ \gamma_2/r - 2\gamma_2\, e^{-\xi} R^{-1} + O(R^{-2}) & \text{for } \beta = -1, \end{cases}$$

which means that we have a weaker boundary layer.

Typical velocity profiles $V(r)$ for various R, as well as the corresponding asymptotic profiles given by (16), are shown in Fig. 1. Evidently, the asymptotic formula produces good approximations to the exact profile even for $R = 20$.

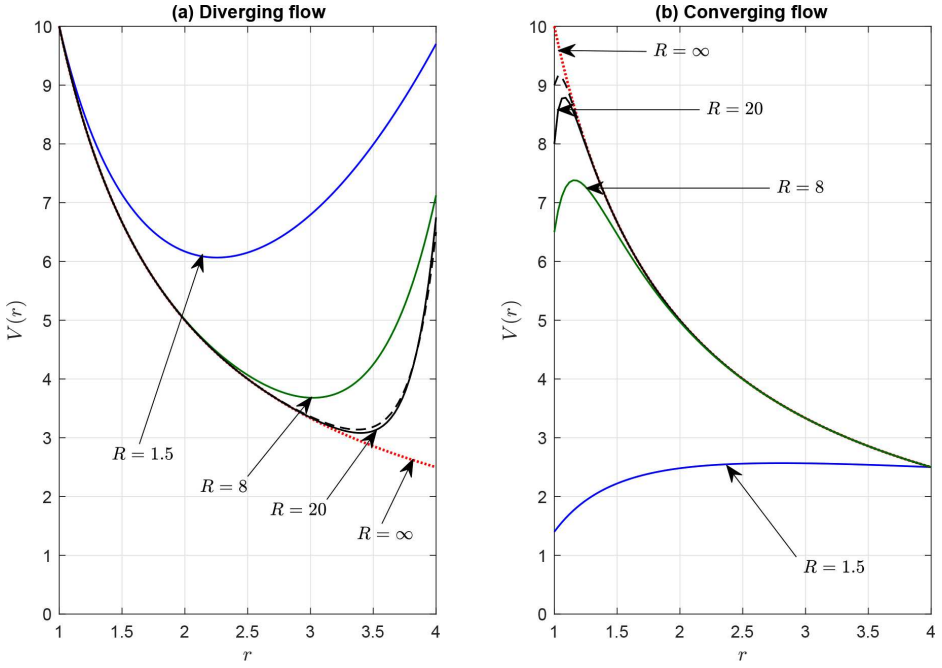

FIG. 1. Typical velocity profiles for $a = 4$ and $R = 1.5, 8, 20$. (a) corresponds to the diverging flow ($\beta = 1$) with $\gamma_1 = 10$ and $s_0 = 1$. (b) corresponds to the converging flow ($\beta = -1$) with $\gamma_2 = 10$ and $s_0 = 1$. Dotted curves represent the inviscid velocity profiles. Dashed curves show $V(r)$ computed using the asymptotic formulas (16) for $R = 20$.

2. The pressure-no-slip conditions

In this case, the azimuthal velocity profile is the same as the one considered in Ref. 13. Constants A and B can be written as

$$A = \frac{\gamma_2 - \gamma_1}{a^{\beta R+2} - 1}, \quad B = \frac{a^{\beta R+2}\gamma_1 - \gamma_2}{a^{\beta R+2} - 1}. \tag{17}$$

The steady solution depends on γ_1, γ_2, and βR and is well defined for all $\beta R \neq -2$. For $\beta R = -2$, the solution is given by Eq. (15) with

$$\tilde{A} = \frac{\gamma_2 - \gamma_1}{\ln a}, \quad \tilde{B} = \gamma_1.$$

The asymptotic formula for $R \gg 1$ is

$$V(r) = \begin{cases} \gamma_1/r + ((\gamma_2 - \gamma_1)/a)e^{-\eta} + O(R^{-1}) & \text{if } \beta = 1, \\ \gamma_2/r - (\gamma_2 - \gamma_1)e^{-\xi} + O(R^{-1}) & \text{if } \beta = -1, \end{cases}$$

where the boundary layer variables ξ and η are the same as before: $\xi = R(r-1)$ and $\eta = R(1 - r/a)$.

Remark 1 (*on the limit* $R \to 0$). To consider the classical Couette flow, we need to pass to the limit $R \to 0$. We cannot simply set $R = 0$ in Eqs. (12) and (17) because of the non-dimensionalization adopted above (which is very convenient for flows with a nonzero radial flux, but not for the classical Couette flow). Thus, we assume that $\gamma_1 \neq 0$ and re-scale the dimensionless quantities in (1)–(11) as

$$t \to t/\gamma_1, \quad \mathbf{v} \to \gamma_1 \mathbf{v}, \quad p \to \gamma_1^2 p.$$

Note that this re-scaling is equivalent to a non-dimensionalization with the azimuthal velocity of the basic flow at the inner cylinder, V_1^*, as the characteristic scale for the velocity, r_1 as the length scale, r_1/V_1^* as the timescale, and $\rho(V_1^*)^2$ as the characteristic scale for the pressure. As a result of this re-scaling, the radial Reynolds number R in (1), (2), and (6)–(11) is replaced by the azimuthal Reynolds number,

$$Re_1 = \gamma_1 R = \frac{V_1^* r_1}{\nu}. \tag{18}$$

If $\gamma_1 = 0$, a similar re-scaling can be done with γ_1 replaced by γ_2. This results in the appearance of the second azimuthal Reynolds number,

$$Re_2 = \gamma_2 R = \frac{V_2^* r_2}{\nu}, \tag{19}$$

where V_2^* is the azimuthal velocity in the basic flow at the outer cylinder. In both cases, we end up with the classical circular Couette flow profile,

$$V(r) = Ar + B/r,$$

with appropriate constants A and B.

From now on, we study the stability of the above steady flows. The corresponding problem for the reference boundary conditions has been studied in detail in Ref. 13. In what follows, all facts concerning the reference boundary conditions are taken from that paper.

D. Linear stability problem

Consider a small perturbation $(\tilde{u}, \tilde{v}, \tilde{p})$ in the form of the normal mode,

$$\{\tilde{u}, \tilde{v}, \tilde{p}\} = \mathrm{Re}\big[\{\hat{u}(r), \hat{v}(r), \hat{p}(r)\}e^{\sigma t + in\theta}\big],$$

where $n \in \mathbb{Z}$. This leads to the following linearized equations:

$$\begin{aligned} K\hat{u} - \frac{\beta}{r^2}\hat{u} - \frac{2V_\beta}{r}\hat{v} &= -\partial_r \hat{p} + \frac{1}{R}\left(L\hat{u} - \frac{\hat{u}}{r^2} - \frac{2in}{r^2}\hat{v}\right), \\ K\hat{v} + \frac{\beta}{r^2}\hat{v} + \Omega_\beta \hat{u} &= -\frac{in}{r}\hat{p} + \frac{1}{R}\left(L\hat{v} - \frac{\hat{v}}{r^2} + \frac{2in}{r^2}\hat{u}\right), \\ \partial_r(r\hat{u}) + in\hat{v} &= 0. \end{aligned} \tag{20}$$

In Eq. (20), V_β with $\beta = \pm 1$ is the azimuthal velocity for the diverging ($\beta = 1$) and converging ($\beta = -1$) flows, $\Omega_\beta(r) = V_\beta'(r) + V_\beta(r)/r$, and

$$K = \sigma + \frac{inV_\beta}{r} + \frac{\beta}{r}\frac{d}{dr}, \quad L = \frac{d^2}{dr^2} + \frac{1}{r}\frac{d}{dr} - \frac{n^2}{r^2}.$$

At the inlet, the boundary conditions for Eq. (20) are

$$\hat{u}(1) = 0, \quad \hat{v}(1) = 0 \tag{21}$$

for $\beta = 1$ and

$$\hat{u}(a) = 0, \quad \hat{v}(a) = 0 \tag{22}$$

for $\beta = -1$. At the outlet, the boundary conditions are either the pressure-stress conditions [that follow from Eqs. (6)–(9)],

$$\hat{p}(a) = \frac{2}{R}\hat{u}'(a), \quad \frac{in}{a}\hat{u}(a) + \hat{v}'(a) - \frac{1}{a}\hat{v}(a) = 0 \tag{23}$$

for $\beta = 1$ and

$$\hat{p}(1) = \frac{2}{R}\hat{u}'(1), \quad in\hat{u}(1) + \hat{v}'(1) - \hat{v}(1) = 0 \tag{24}$$

for $\beta = -1$, or the pressure-no-slip conditions

$$\hat{p}(a) = \frac{2}{R}\hat{u}'(a), \quad \hat{v}(a) = 0 \tag{25}$$

for $\beta = 1$ and

$$\hat{p}(1) = \frac{2}{R}\hat{u}'(1), \quad \hat{v}(1) = 0 \tag{26}$$

for $\beta = -1$.

It can be shown that if we restrict our analysis to axisymmetric perturbations, then the basic steady flow (12) is asymptotically stable not only to small perturbations but also to perturbations of arbitrary amplitude. For the sake of completeness, the proof of this fact is given in Appendix A. In particular, it implies that the mode with $n = 0$ cannot be unstable for any value of the Reynolds number. Thus, we shall consider only the modes with $n \neq 0$.

In terms of stream function $\hat{\psi}(r)$, such that $\hat{u} = \frac{in}{r}\hat{\psi}(r)$ and $\hat{v} = -\hat{\psi}'(r)$, the first two equations (20) are replaced by the vorticity equation,

$$\left(\sigma + \frac{inV_\beta}{r} + \frac{\beta}{r}\partial_r\right)L\hat{\psi} - \frac{in}{r}\Omega_\beta'(r)\hat{\psi} = R^{-1}L^2\hat{\psi}. \tag{27}$$

The inlet boundary conditions become

$$\hat{\psi}(1) = 0, \quad \hat{\psi}'(1) = 0 \quad \text{for } \beta = 1, \tag{28}$$

$$\hat{\psi}(a) = 0, \quad \hat{\psi}'(a) = 0 \quad \text{for} \quad \beta = -1. \tag{29}$$

To find the pressure, we employ the second equation (20). As a result, we have

$$\hat{p} = \frac{ir}{nR}\left(L\hat{\psi}_r - \frac{\hat{\psi}_r}{r^2} + \frac{2n^2}{r^3}\,\hat{\psi}\right) - \frac{ir}{n}\left[\left(\sigma + \frac{inV_\beta}{r} + \frac{\beta}{r}\,\partial_r\right)\hat{\psi}_r + \frac{\beta}{r^2}\,\hat{\psi}_r - \frac{in}{r}\,\Omega_\beta\,\hat{\psi}\right]. \tag{30}$$

Thus, the normal stress conditions at the outlet [the first equations in (23)–(26)] can be written as

$$\left[\frac{1}{R}\left(L\hat{\psi}_r - \frac{1+2n^2}{r^2}\,\hat{\psi}_r + \frac{4n^2}{r^3}\,\hat{\psi}\right) - \left(\sigma + \frac{inV_1}{r} + \frac{1}{r}\,\partial_r\right)\hat{\psi}_r - \frac{1}{r^2}\,\hat{\psi}_r + \frac{in}{r}\,\Omega_1\,\hat{\psi}\right]\Bigg|_{r=a} = 0 \tag{31}$$

for $\beta = 1$ and

$$\left[\frac{1}{R}\left(L\hat{\psi}_r - \frac{1+2n^2}{r^2}\,\hat{\psi}_r + \frac{4n^2}{r^3}\,\hat{\psi}\right) - \left(\sigma + \frac{inV_{-1}}{r} - \frac{1}{r}\,\partial_r\right)\hat{\psi}_r + \frac{1}{r^2}\,\hat{\psi}_r + \frac{in}{r}\,\Omega_{-1}\,\hat{\psi}\right]\Bigg|_{r=1} = 0 \tag{32}$$

for $\beta = -1$. The tangent stress conditions at the outlet [the second equations in (23) and (24)] take the following form:

$$\hat{\psi}''(a) - \frac{1}{a}\,\hat{\psi}'(a) + \frac{n^2}{a^2}\,\hat{\psi}(a) = 0 \quad \text{for} \quad \beta = 1, \tag{33}$$

$$\hat{\psi}''(1) - \hat{\psi}'(1) + n^2\hat{\psi}(1) = 0 \quad \text{for} \quad \beta = -1. \tag{34}$$

The no-slip conditions at the outlet [given by the second equations in (25) and (26)] become

$$\hat{\psi}'(a) = 0 \quad \text{for} \quad \beta = 1, \quad \hat{\psi}'(1) = 0 \quad \text{for} \quad \beta = -1. \tag{35}$$

Note that, in view of (35), conditions (31) and (32) simplify to

$$\left[\frac{1}{R}\left(\hat{\psi}_{rrr} + \frac{1}{r}\,\hat{\psi}_{rr} + \frac{4n^2}{r^3}\,\hat{\psi}\right) - \frac{1}{r}\,\hat{\psi}_{rr} + \frac{in}{r}\,\Omega_1\,\hat{\psi}\right]\Bigg|_{r=a} = 0 \tag{36}$$

for $\beta = 1$ and

$$\left[\frac{1}{R}\left(\hat{\psi}_{rrr} + \frac{1}{r}\,\hat{\psi}_{rr} + \frac{4n^2}{r^3}\,\hat{\psi}\right) + \frac{1}{r}\,\hat{\psi}_{rr} + \frac{in}{r}\,\Omega_{-1}\,\hat{\psi}\right]\Bigg|_{r=1} = 0 \tag{37}$$

for $\beta = -1$.

Simply by looking at Eqs. (12)–(17) and (27)–(35), one can deduce the following. First, for a given β, an eigenvalue is a function of five parameters: $\sigma = \sigma(a, n, \gamma_1, \gamma_2, R)$ in the case of the pressure-no-slip conditions; $\sigma = \sigma(a, n, \gamma_\alpha, s_0, R)$, with $\alpha = 1$ for $\beta = 1$ and $\alpha = 2$ for $\beta = -1$, in the case of the pressure-stress conditions. Second, if $\sigma(a, n, \gamma_1, \gamma_2, R)$ [or $\sigma(a, n, \gamma_\alpha, s_0, R)$] is an eigenvalue, then so are $\bar{\sigma}(a, -n, \gamma_1, \gamma_2, R)$ [or $\bar{\sigma}(a, -n, \gamma_\alpha, s_0, R)$] and $\sigma(a, -n, -\gamma_1, -\gamma_2, R)$ [or $\sigma(a, -n, -\gamma_\alpha, -s_0, R)$]. Here, $\bar{\sigma}$ is the complex conjugate of σ. These properties imply that it suffices to consider only positive n and, also, a certain symmetry of the neutral curves (which will be used later).

For $R \gg 1$, an asymptotic theory of the eigenvalue problems with the pressure–stress or pressure-no-slip conditions can be developed along the same lines as in Ref. 13. In particular, it can be shown that both problems reduce to an inviscid spectral problem, which will be briefly discussed in Sec. III. We note in passing that this is a nontrivial property because of the following two facts: (i) the basic viscous flow depends on the Reynolds number R and (ii) a single inviscid steady flow represents a vanishing viscosity limit for continuous families of viscous steady flows [given by Eqs. (12)–(17)].

III. INVISCID STABILITY PROBLEM

In the inviscid limit ($R \to \infty$), Eq. (27) simplifies to

$$\left(\sigma + \frac{in\gamma_\alpha}{r^2} + \frac{\beta}{r}\,\partial_r\right)L\hat{\psi} = 0, \tag{38}$$

where $\alpha = 1$ if $\beta = 1$ and $\alpha = 2$ if $\beta = -1$. Boundary conditions at the inlet remain the same,

$$\hat{\psi}(1) = 0, \quad \hat{\psi}'(1) = 0 \tag{39}$$

for the diverging flow ($\beta = 1$) and

$$\hat{\psi}(a) = 0, \quad \hat{\psi}'(a) = 0 \tag{40}$$

for the converging flow ($\beta = -1$).

At the outlet, the normal stress conditions (31) and (32) reduce to

$$\left[\left(\sigma + \frac{in\gamma_1}{r^2} + \frac{1}{r}\,\partial_r\right)\hat{\psi}'(r) + \frac{1}{r^2}\,\hat{\psi}'(r)\right]\Bigg|_{r=a} = 0 \tag{41}$$

for $\beta = 1$ and

$$\left[\left(\sigma + \frac{in\gamma_2}{r^2} - \frac{1}{r}\,\partial_r\right)\hat{\psi}'(r) - \frac{1}{r^2}\,\hat{\psi}'(r)\right]\Bigg|_{r=1} = 0 \tag{42}$$

for $\beta = -1$, and the tangent stress conditions (33) and (34) and the no-slip conditions (35) must be discarded (as irrelevant for the inviscid fluid). Conditions (41) and (42) imply that the perturbation pressure $\hat{p}(r)$ must be zero at the outlet. Thus, we shall call them the pressure conditions.

Equations (38)–(42) represent eigenvalue problems for σ arising in the stability analysis of the steady inviscid diverging and converging inviscid flows, given by

$$u = \frac{\beta}{r}, \quad v = \frac{\gamma_\alpha}{r}. \tag{43}$$

In these problems, we can analytically derive dispersion relations for σ.

A. Diverging flow ($\beta = 1$)

For $\beta = 1$, eigenvalues σ satisfy the dispersion relation $D(\sigma, n, a, \gamma_1) = 0$ with

$$D \equiv \left(a^2\sigma + in\gamma_1 + n\right)a^{n-3}\,I_1 + \left(a^2\sigma + in\gamma_1 - n\right)a^{-(n+3)}\,I_2 + \frac{2}{a}\,e^{-g_1(a)}, \tag{44}$$

where $g_1(r) = \sigma r^2/2 + in\gamma_1 \ln r$ and

$$I_1 = \int_1^a r^{-n+1}\, e^{-g_1(r)}\, dr, \quad I_2 = \int_1^a r^{n+1}\, e^{-g_1(r)}\, dr. \tag{45}$$

Evidently, the dispersion relation has the following properties:

$$\overline{D(\sigma, n, a, \gamma_1)} = D(\bar{\sigma}, -n, a, \gamma_1),$$
$$D(\sigma, -n, a, -\gamma_1) = D(\sigma, n, a, \gamma_1).$$

(Here "bar" denotes complex conjugation.) These properties imply that we need to consider only positive n and γ_1.

Numerical evaluation of the dispersion relation shows that there are no eigenvalues with positive real parts if $\gamma_1 = 0$. If γ_1 increases from 0, the roots of Eq. (44) move on the complex plane and, at some critical value, $\gamma_1 = \gamma_{1cr}$, one of the eigenvalues crosses the imaginary axis, so that for $\gamma_1 > \gamma_{1cr}$, there is an eigenvalue with a positive real part, and hence, the flow is unstable.

Numerical calculations produced the stability diagram presented in Fig. 2. It shows neutral curves on the (a, γ_1) plane for normal modes with $n = 1, \ldots, 6$. The instability region for each mode is above the corresponding curve. Solid curves correspond to the pressure condition (41), and dashed curves correspond to the normal velocity condition (which sets the normal velocity perturbation at the outlet to zero). For all curves in Fig. 2, $\mathrm{Im}(\sigma) \neq 0$, i.e., the instability is oscillatory, and neutral modes are periodic traveling azimuthal waves.

Although the neutral curves in both problems look qualitatively similar, there are two interesting differences, namely,

(i) For each azimuthal mode, the curve for the pressure condition is below the one corresponding to the normal velocity condition, which means that the same flow is more unstable if the pressure condition is used, and the gap between each pair of curves corresponding to the same n is larger for smaller a.

(ii) For the normal velocity condition, the critical value of γ_1 is a monotonically decreasing function of a, for all azimuthal modes. However, in the case of the pressure condition, the neutral curves for modes with higher azimuthal wave numbers (for $n = 3, \ldots, 6$) have a local minimum, and the minimum is attained at smaller values of a for higher n.

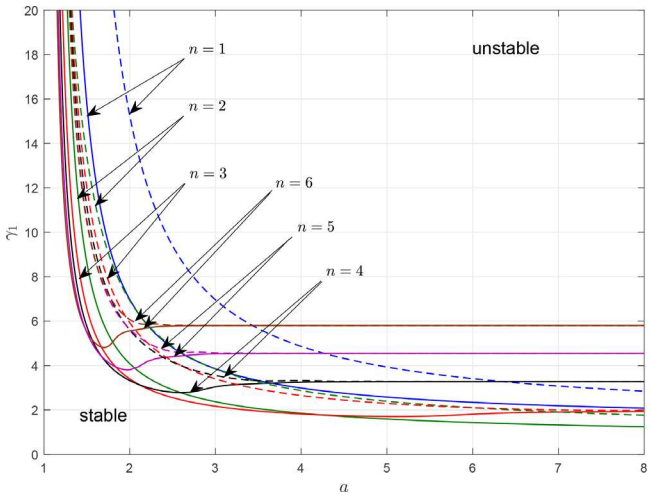

FIG. 2. Diverging flow: solid curves represent neutral curves for azimuthal modes with $n = 1, \ldots, 6$; dashed curves show neutral curves for the normal velocity condition, taken from Ref. 12.

It should be mentioned here that, motivated by an application to a flow in a radial vaneless diffusor, the stability of the diverging flow [given by Eq. (43) with $\beta = 1$] has been recently studied in Ref. 22. Although the paper contains several typos/errors (most notably, in the dispersion relation), the neutral curves presented there seem to agree with the curves in Fig. 2.

Remark 2 (*on the limit of weak radial flow*). It can be shown that, in the limit $\gamma_1 \to \infty$,

$$\sigma = -in\gamma_1 + \gamma_1^{1/2}\left(\lambda + O(\gamma_1^{-1/2})\right),$$

where λ is a root of the equation

$$\int_0^\infty e^{-\lambda x + inx^2}\, dx = 0.$$

The corresponding eigenfunction is given by

$$\hat{\phi}(r) = \left[F(\xi) - \frac{F(0) r^n}{1 + a^{2n}}\left(1 + a^{2n}/r^{2n}\right)\right],$$

where

$$F(\xi) = \int_\xi^\infty (x - \xi) e^{-\lambda x + inx^2}\, dx, \quad \xi = \gamma_1^{1/2}(r - 1).$$

The derivation of this approximation simply repeats the arguments laid down in Ref. 12 (see also Ref. 10) for the case of the normal velocity conditions.

It turns out that the leading-order approximations to σ are the same for both the pressure condition and the normal velocity condition. This suggests that, for $\gamma_1 \gg 1$, the instability has the same mechanism in both problems. This, however, does not mean that the change in the boundary condition at the outlet has little effect at all values of γ_1. Indeed, the neutral curves are notably different in these two problems, as one can see in Fig. 2.

B. Converging flow ($\beta = -1$)

The dispersion relation for the converging flow is given by

$$\tilde{D}(\sigma, n, a, \gamma_2) \equiv (\sigma + in\gamma_2 - n)\tilde{I}_1 + (\sigma + in\gamma_2 + n)\tilde{I}_2 + 2\, e^{g_2(1)} = 0, \tag{46}$$

where $g_2(r) = \sigma r^2/2 + in\gamma_2 \ln r$ and

$$\tilde{I}_1 = \int_1^a r^{-n+1}\, e^{g_2(r)}\, dr, \quad \tilde{I}_2 = \int_1^a r^{n+1}\, e^{g_2(r)}\, dr. \tag{47}$$

Evidently, it has the same properties as those for the diverging flow,

$$\overline{\tilde{D}(\sigma, n, a, \gamma_2)} = \tilde{D}(\bar{\sigma}, -n, a, \gamma_2),$$
$$\tilde{D}(\sigma, -n, a, -\gamma_2) = \tilde{D}(\sigma, n, a, \gamma_2).$$

Again, these imply that we need to consider only positive n and γ_2.

The neutral curves on the (a, γ_2) plane for modes with $n = 1, \ldots, 6$ are shown in Fig. 3. The instability region for each mode is above the corresponding curve. As before, the solid curves represent neutral curves for the pressure condition, and the dashed curves are curves for the normal velocity condition.[12] Qualitatively, the only difference between Figs. 2 and 3 is that every neutral curve in the latter has a local minimum. Conclusions (i) and (ii) and the remark on the limit of weak radial flow made for the diverging flows are also true for the converging flows.

Remark 3 (*on three-dimensional perturbations*). To further justify our hypothesis that the two-dimensional theory may describe observable phenomena in this problem, consider the stability of the diverging inviscid flows to three-dimensional perturbations. In the 3D case, a small perturbation is assumed to have the form $\{\tilde{u}, \tilde{v}, \tilde{w}, \tilde{p}\} = \mathrm{Re}[\{\hat{u}(r), \hat{v}(r), \hat{w}(r), \hat{p}(r)\}e^{\sigma t + in\theta + ikz}]$, where $\tilde{w}$ is the axial component of the perturbation velocity, and $k > 0$ is the axial wave number. This leads to the following dispersion relation for σ: $D(\sigma, n, k, a, \gamma_1) = 0$, where

$$D = k\left(a\sigma + \frac{in\gamma_1}{a}\right)J_1 + k^2 J_2 + a\, e^{-g_1(a)},$$

$$J_1 = \int_1^a \left[I_n'(ks)K_n(ka) - I_n(ka)K_n'(ks)\right] e^{-g_1(s)} s^2\, ds, \tag{48}$$

$$J_2 = \int_1^a \left[I_n'(ks)K_n'(ka) - I_n'(ka)K_n'(ks)\right] e^{-g_1(s)} s^2\, ds.$$

Here, $I_n(z)$ and $K_n(z)$ are the modified Bessel functions of the first and second kind. It can be shown that in the limit $k \to 0$, it reduces to the two-dimensional dispersion relation, given by (44) and (45).

Critical values of γ_1 vs the axial wave number k for $a = 2$ are shown in Fig. 4 (solid curves). The dashed curves represent neutral curves for the normal velocity condition.[14] Figure shows that for all

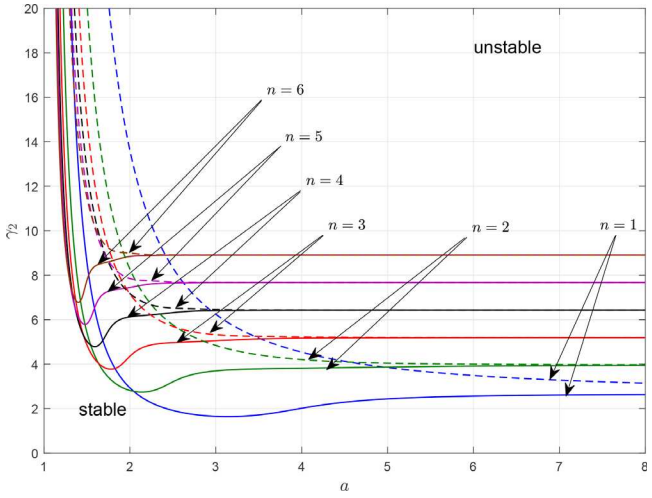

FIG. 3. Converging flow: solid curves represent neutral curves for azimuthal modes with $n = 1, \ldots, 6$; dashed curves show the results for the normal velocity conditions, obtained from Ref. 12.

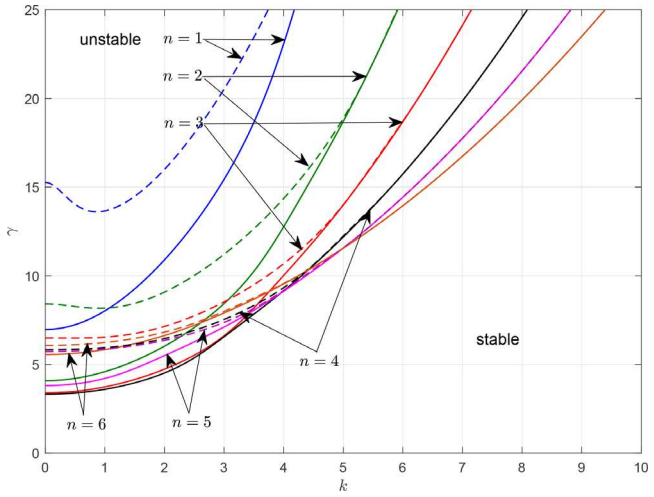

FIG. 4. Neutral curves for three-dimensional modes for the diverging flow with $a = 2$ and $n = 1, \ldots, 6$; dashed curves show the results for the normal velocity conditions.[14]

azimuthal modes, the minimum critical value of γ_1 is attained at $k = 0$, i.e., for two-dimensional modes. Note that this is not so in the case of normal velocity conditions where, for lower modes ($n = 1, 2$), the minimum is attained at a finite value of k. Nevertheless, the most unstable perturbation (minimized over all n) is two-dimensional in both cases.

It is also clearly seen that for k of order unity and smaller, the pressure condition has destabilizing effect (in comparison with the normal velocity condition). For large k (short axial waves), the neutral curves for both conditions almost coincide. This is consistent with an earlier asymptotic result[14] that for $k \gg 1$, the eigenfunctions are concentrated near the inlet ($r = 1$) and do not depend on the boundary condition at the outlet ($r = a$).

We have not computed neutral curves for other values of a and for the converging flows. However, the general patterns of what we can see here and what was observed earlier[14] for the normal velocity condition look very similar, so that it is reasonable to expect that for converging flows as well as for other values of a, the two-dimensional modes will remain to be the most unstable ones.

In Sec. IV, we shall describe the results of solving the viscous stability problem numerically.

IV. VISCOUS STABILITY RESULTS

A. Numerical method

The eigenvalue problems with the pressure-stress and pressure-no-slip conditions are solved numerically using the Galerkin method with polynomial basis functions based on Legendre polynomials. For the problem with the pressure-stress conditions, the basis functions are chosen to satisfy the boundary conditions at the inlet, given by Eq. (28) or (29), and at the outlet by (33) or (34). Thus, $\hat{\psi}$ is approximated by

$$\hat{\psi}(r) = \sum_{k=0}^{N} c_k \phi_k(x), \quad x = -1 + \frac{2}{a-1}(r-1),$$

with basis functions $\phi_k(x)$, given by

TABLE I. The difference between the eigenvalues with the largest real part computed using the Galerkin method (σ_G) and the shooting method (σ_S): the diverging flow for $a=2$, $n=1$, and $\gamma_1 = 10$ with $s_0 = 0$ for the pressure-stress conditions and $\gamma_2 = 0$ for the pressure-no-slip conditions.

	Pressure-stress conditions			Pressure-no-slip conditions		
R	40	100	500	40	100	500
$\lvert\sigma_G - \sigma_S\rvert$	3.3352×10^{-9}	1.2040×10^{-9}	5.1103×10^{-10}	1.4622×10^{-7}	8.2404×10^{-8}	1.4389×10^{-7}

$$\phi_k(x) = \begin{cases} (1+x)^2(x+\lambda_k)P_k(x) & \text{for } \beta = 1, \\ (1-x)^2(x+\lambda_k)P_k(x) & \text{for } \beta = -1, \end{cases}$$

for $k = 0, \ldots, N$, where $P_k(x)$ is the Legendre polynomial of degree k and λ_k is a constant chosen so as to satisfy (33) or (34) [note that conditions (28) or (29) are automatically satisfied]. The normal stress condition, given by Eq. (31) or (32), is satisfied using the τ-method (see, e.g., Ref. 34).

In the case of the pressure-no-slip conditions, the τ-method yields spurious eigenvalues because conditions (36) and (37) do not contain the spectral parameter σ. However, the same fact makes it possible to construct basis functions that satisfy all the boundary conditions. These basis functions have the following form:

$$\phi_k(x) = \begin{cases} (1+x)^2(x^2+\lambda_k x+\delta_k)P_k(x) & \text{for } \beta = 1, \\ (1-x)^2(x^2+\lambda_k x+\delta_k)P_k(x) & \text{for } \beta = -1, \end{cases}$$

where constants λ_k and δ_k are chosen to satisfy the conditions given by the first Eqs. (35) and (36) if $\beta = 1$ and the second Eqs. (35) and (37) if $\beta = -1$.

To verify the method, some of the computed eigenvalues were compared with eigenvalues obtained using the shooting method. Table I displays the difference between eigenvalues computed using the Galerkin method and the shooting method for the diverging flows for $a=2$, $n=1$, $\gamma_1 = 10$, $s_0 = 0$ for the pressure-stress conditions, and $\gamma_2 = 0$ for the pressure-no-slip conditions and for several values of the radial Reynolds number. The number of basis functions in the Galerkin method was $N=100$. The table shows that the difference is very small for both types of boundary conditions. Further verification was provided by checking the consistency of the results for high radial Reynolds numbers with the inviscid theory of Sec. III. Figure 5 shows how neutral curves for the diverging flow with the pressure-no-slip conditions approach the critical values of γ_1 (computed using the inviscid theory) in the limit $R \to \infty$. In Fig. 5, solid lines represent neutral curves for $a=2$, $\gamma_2 = 0$, and $n = 1, \ldots, 5$, and the vertical dashed lines correspond to critical values of γ_1 from the inviscid theory. Evidently, each neutral curves approach the relevant inviscid limit as $R \to \infty$, which shows that the numerical method produces results consistent with the inviscid theory of Sec. III.

In most calculations, the number of basis functions was in the range from $N=100$ to $N=200$. To check the convergence of the numerical algorithm, we performed a few calculations with a double number of basis functions for each curve shown in Figs. 7–17 and increased N whenever the results showed the dependence on N. To demonstrate that $N=100$ is enough to capture the boundary layer behavior of eigenfunctions at least for $R \approx 1000$, we plotted real and imaginary parts of $\hat{v}(r) = -\hat{\psi}'(r)$ for neutral modes for the diverging and converging flows with the pressure-no-slip boundary conditions in Fig. 6. In Fig. 6, panel (a) shows real (solid curves) and imaginary (dashed curves) parts of $\hat{v}(r)$ for the diverging flow with $a=2$, $n=3$, $\gamma_1 = 3.414$, $\gamma_2 = 0$, $R=1002.8$, and $\sigma = -1.6496i$; panel (b) is a magnified part of (a) near $r=2$; panel (c) shows real (solid curves) and imaginary (dashed curves) parts of $\hat{v}(r)$ for the converging flow with $a=2$, $n=1$, $\gamma_1 = 0$, $\gamma_2 = 3$, $R=1002.9$, and $\sigma = -0.413\,08i$; and panel (d) is a magnified part of (c) near $r=1$. Evidently, the eigenfunctions display boundary layer behavior at the outlet, as expected, and the spatial resolution of the numerical method is sufficient to accurately reproduce boundary layers. Note also that thickness of the boundary layer for the diverging flow [panel (b)] looks twice larger than that for the converging flows [panel (d)]. This is consistent with the fact that the boundary layer thickness for the diverging flow is $O(a/R)$, compared with $O(1/R)$ for the converging flow, as follows from the definition of the boundary layer variables η and ξ in Sec. III A.

B. Problem with the pressure–stress conditions

1. Diverging flow

Figures 7 and 8 show neutral curves on the (γ_1, R) plane for $a=2$ and $a=8$, respectively. The solid curves correspond to the pressure–stress conditions with $s_0 = 0$. The dashed curves are neutral curves for the reference boundary conditions with $\gamma_2 = 0$, obtained in Ref. 13. All curves in Figs. 7 and 8 approach vertical asymptotes as γ_1 tends to $\gamma_1^*(a,n)$ from the right, where $\gamma_1^*(a,n)$ is the critical value of γ_1 for the inviscid mode with azimuthal number n. Numbers $\gamma_1^*(a,n)$ can be determined from the inviscid diagram shown in Fig. 2.

We note in passing that, in view of the symmetry properties of the eigenvalue problem, critical curves for negative γ_1 can be obtained by reflecting the curves in Figs. 7 and 8 about the vertical axis.

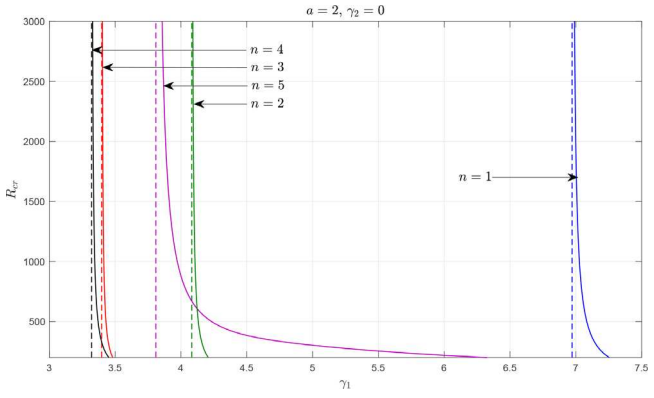

FIG. 5. Neutral curves for $R \gg 1$ for the diverging flow with the pressure-no-slip conditions (solid curves): $a=2$, $\gamma_2 = 0$, and $n = 1, \ldots, 5$. The dashed lines correspond to critical values of γ_1 in the inviscid theory.

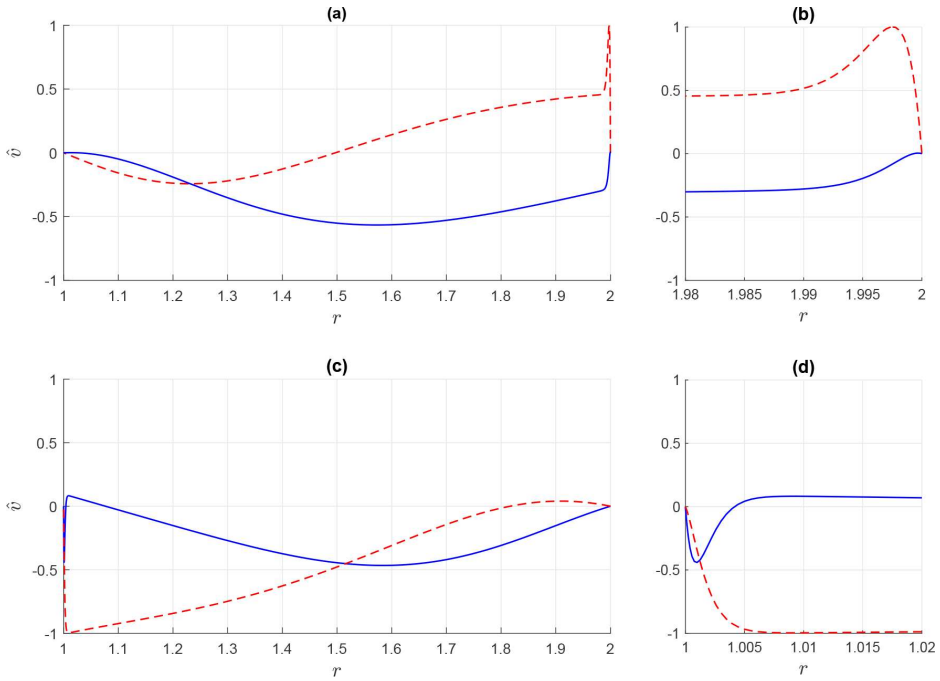

FIG. 6. Eigenfunctions $\hat{v}(r) = -\hat{\psi}'(r)$ for neutral modes with pressure-no-slip conditions (solid curves—Re $\hat{v}$, dashed curves—Im $\hat{v}$). (a) and (b) Diverging flow for $a = 2$, $n = 3$, $\gamma_1 = 3.414$, $\gamma_2 = 0$, and $R = 1002.8$; (b) shows a magnified part of (a) near $r = a$. (c) and (d) Converging flow for $a = 2$, $n = 1$, $\gamma_1 = 0$, $\gamma_2 = 3$, and $R = 1002.9$; (d) is a magnified part of (c) near $r = 1$.

Figure 7 shows that the critical curves for $a = 2$ are below the corresponding curves for the problem with the reference boundary conditions, and the gap between the curves with the same azimuthal wave number n is larger for smaller n and decreases when n increases. The same is true for the critical curves for $a = 8$, but the effect is much weaker: one can see in Fig. 8 that the gap between the curves with $n = 1$ is much smaller than the corresponding gap for $a = 2$, and it becomes invisible for modes with $n > 1$. We can conclude that the pressure-stress boundary conditions make the flow more unstable, and this effect is stronger for smaller a. The latter is not surprising, as it is natural to expect that for wider annuli the effect of the boundary conditions at the outlet is weaker. Nevertheless, it is a useful observation: It implies that the upstream influence of the pressure-stress conditions becomes much weaker for larger gaps, which justifies using these conditions on artificial boundaries sufficiently distant from a region of interest.

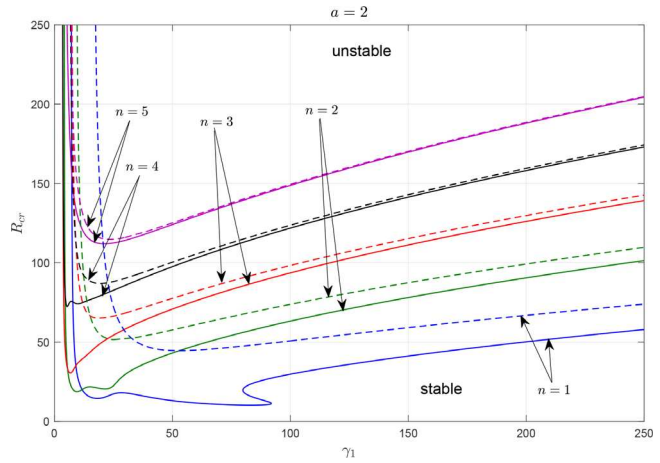

FIG. 7. Diverging flow with the pressure-stress conditions: critical R vs γ_1 for $a = 2$ and $n = 1, \ldots, 5$. Solid curves correspond to the pressure-stress conditions with $s_0 = 0$, and dashed curves correspond to the reference conditions with $\gamma_2 = 0$.

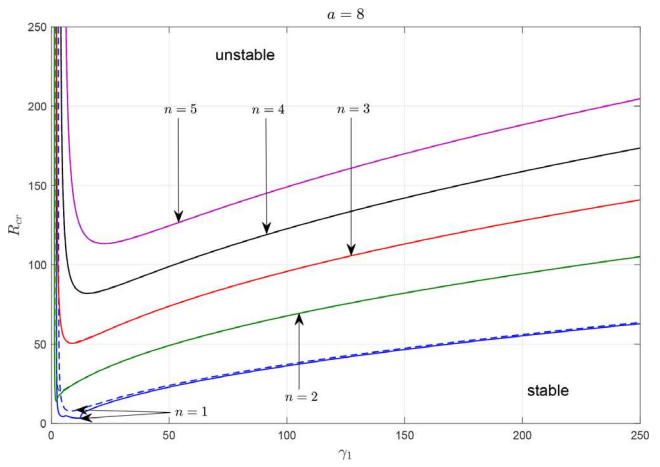

FIG. 8. Diverging flow with the pressure-stress conditions: critical R vs γ_1 for $a = 8$ and $n = 1, \ldots, 5$. Solid curves correspond to the pressure-stress boundary conditions with $s_0 = 0$, and dashed curves correspond to the reference conditions with $\gamma_2 = 0$.

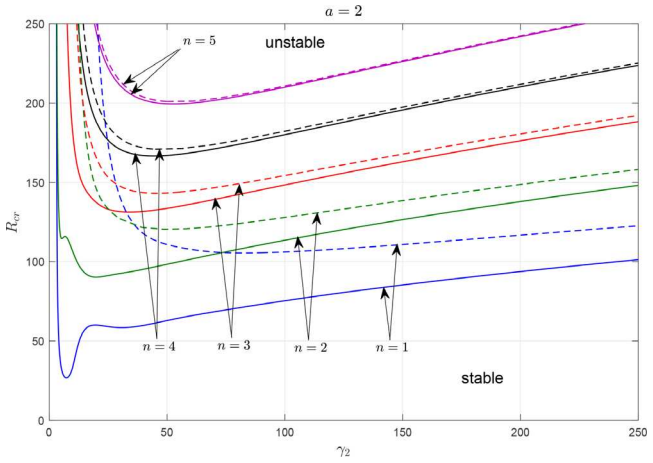

FIG. 9. Converging flow with the pressure-stress conditions: critical R vs γ_2 for $a = 2$ and $n = 1, \ldots, 5$. Solid curves correspond to the pressure-stress conditions with $s_0 = 0$, and dashed curves correspond to the reference boundary conditions with $\gamma_1 = 0$.

2. Converging flow

Figures 9 and 10 show critical curves on the (γ_2, R) plane for the converging flow ($\beta = -1$) for $a = 2$ and $a = 8$. The solid curves correspond to the pressure–stress conditions with $s_0 = 0$, and the dashed curves—to the reference boundary conditions with $\gamma_1 = 0$. Everything that has been said about the diverging flows can also be said about the neutral curves for the converging flows. The only difference is that the critical curves for the converging flows are above the corresponding curves for the diverging flows, i.e., the former is more stable than the latter, but we still have the result that the flows with the pressure–stress conditions are more unstable than those with the reference conditions.

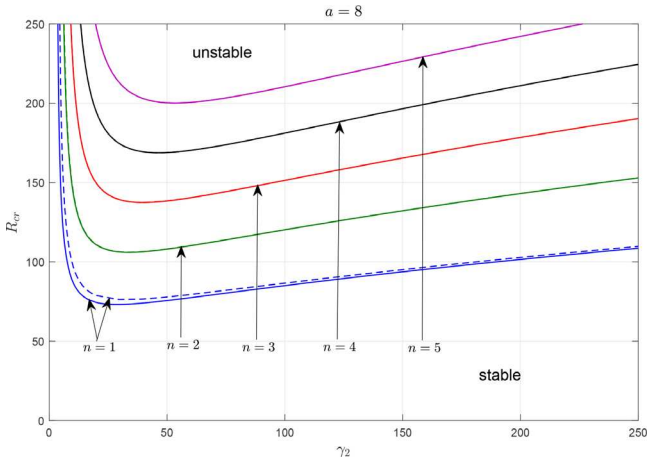

FIG. 10. Converging flow with the pressure-stress conditions: critical R vs γ_2 for $a = 8$ and $n = 1, \ldots, 5$. Solid curves correspond to the pressure-stress boundary conditions with $s_0 = 0$; dashed curves correspond to the reference boundary conditions with $\gamma_1 = 0$.

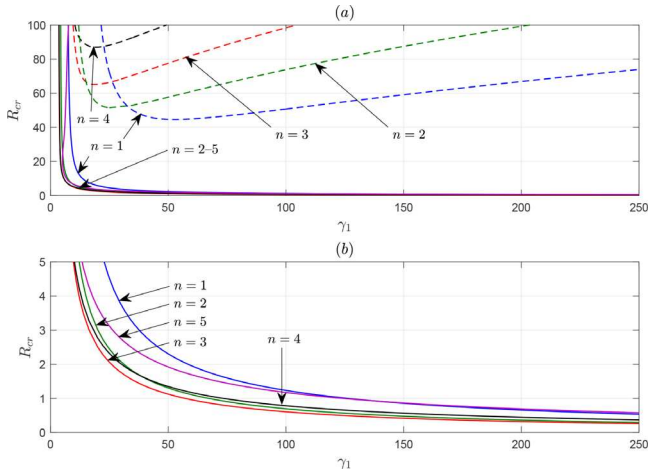

FIG. 11. Diverging flow with the pressure-no-slip conditions: critical R vs γ_1 for $a = 2$, $\gamma_2 = 0$, and $n = 1, \ldots, 5$: (a) solid curves correspond to the pressure-no-slip conditions and dashed curves correspond to the reference boundary conditions; (b) shows a magnified lower part of (a).

C. Problem with the pressure-no-slip conditions

1. Diverging flow

Figures 11(a) and 12(a) display the critical curves for the pressure-no-slip conditions (solid curves), as well as the curves for the reference conditions (dashed curves), for $a = 2$ and $a = 8$. Figures 11(b) and 12(b) show the same curves for small R in more detail. Evidently, as $\gamma_1 \to \infty$, the neutral curves monotonically approach the horizontal line $R = 0$, which suggests that in the limit $\gamma_1 \to \infty$ (equivalently, in the limit of a weak radial flow), the basic flow is unstable for all $R > 0$. This behavior is very different from both the case of the pressure–stress conditions and the case of the reference conditions, for which the critical Reynolds number grows linearly with γ_1 for $\gamma_1 \gg 1$.

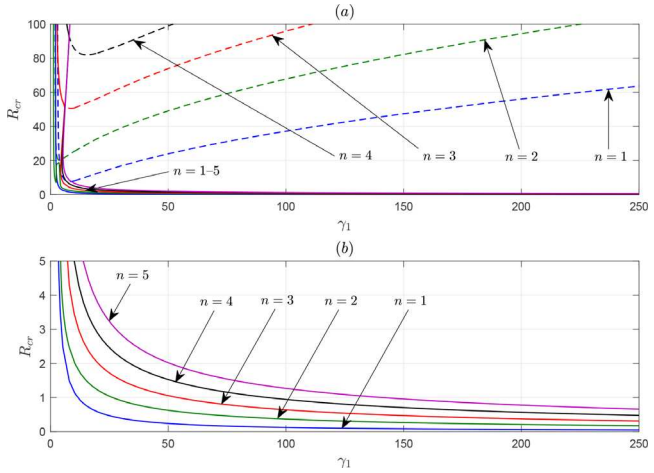

FIG. 12. Diverging flow with the pressure-no-slip conditions: critical R vs γ_1 for $a = 8$, $\gamma_2 = 0$, and $n = 1, \ldots, 5$: (a) solid curves correspond to the pressure-no-slip conditions and dashed curves correspond to the reference boundary conditions; (b) shows a magnified lower part of (a).

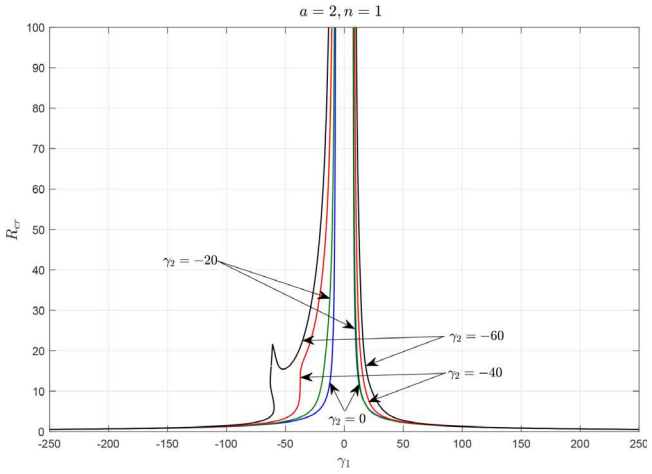

FIG. 13. Diverging flow with the pressure-no-slip conditions: critical R vs γ_1 for $a = 2$, $n = 1$, and $\gamma_2 = 0, -20, -40, -60$.

The critical curves for $a = 2$, $n = 1$ and several values of γ_2 are shown in Fig. 13. While the curve for $\gamma_2 = 0$ is symmetric relative to the vertical axis, the curves for $\gamma_2 \neq 0$ are not symmetric. However, due to the symmetries of the eigenvalue problem mentioned earlier, the critical curves for the same a and n and for $\gamma_2 = 0, 20, 40, 60$ can be obtained by reflecting the curves in Fig. 13 about the vertical axis $\gamma_1 = 0$. Note that, for sufficiently large $|\gamma_1|$, the critical curves for all values of γ_2 approach the axis $R = 0$. Thus, this effect appears to be independent of γ_2. Note also that the dependence of the critical curves on γ_2 (i.e., on what is happening at the outlet) is relatively weak.

It turns out that it is possible to construct an asymptotic approximation of the eigenvalue problem for large γ_1. This is done in Appendix B, where it is shown that, in the leading order, the critical values of R are given by

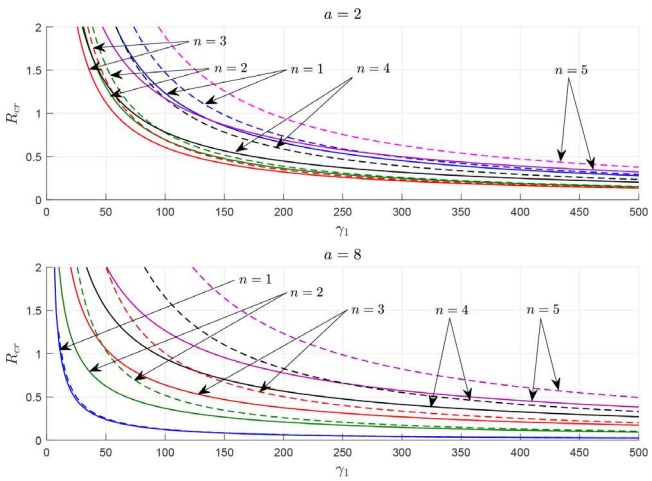

FIG. 14. Diverging flow with the pressure-no-slip conditions: critical R vs γ_1 for large γ_1 for $a = 2$ (upper plot) and $a = 8$ (lower plot). Dashed curves show the leading-order asymptotic values of R_{cr} for $\gamma_1 \gg 1$.

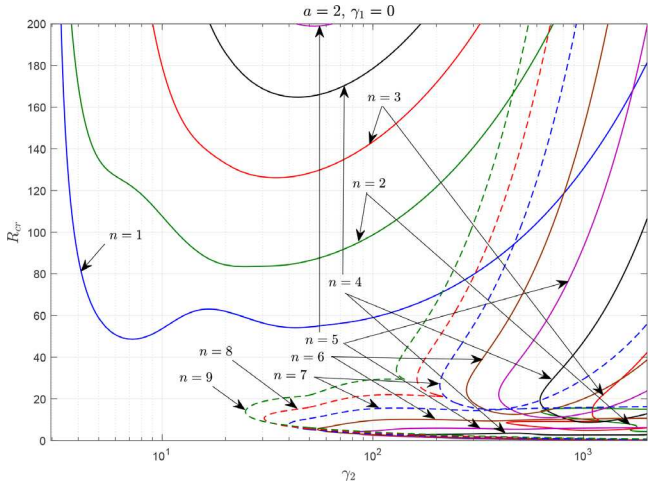

FIG. 15. Converging flow with the pressure-no-slip conditions: critical R vs γ_2 for $a = 2$ and $\gamma_1 = 0$.

$$R_{cr} = \frac{Re_{1cr}(a, n)}{\gamma_1} + O\left(\gamma_1^{-2}\right), \tag{49}$$

where $Re_{1cr}(a, n)$ is a certain critical value of the azimuthal Reynolds number, Re_1, defined by Eq. (18). The leading-order approximations computed using Eq. (49), as well as the critical curves obtained by solving the original eigenvalue problem, are shown as dashed and solid curves, respectively, in Fig. 14. One can see that the dashed curves approach the solid curves as γ_1 increases, which indicates that the asymptotic formula (49), obtained in Appendix B, works. Note also that Re_{1cr} depends only on a and n and does not depend on γ_2, i.e., on the azimuthal velocity at the outlet (of course, higher-order approximations will depend on γ_2). This means that, in the leading order, the asymptotic behavior of the critical curves for $\gamma_2 \neq 0$ is the same as

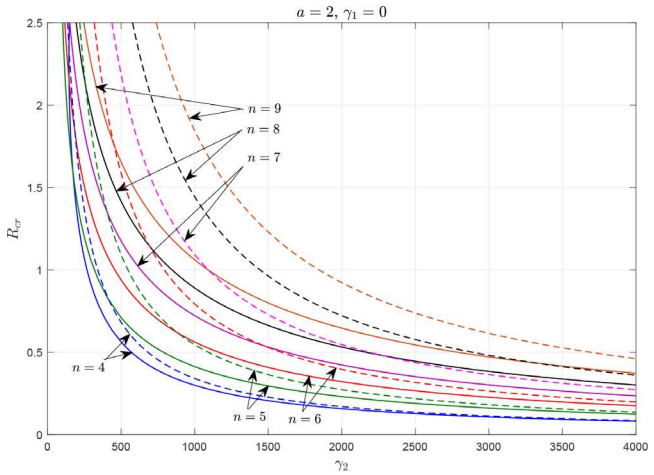

FIG. 16. Converging flow with the pressure-no-slip conditions: critical R vs γ_2 for $\gamma_2 \gg 1$ for $a = 2$, $\gamma_1 = 0$, and $n = 4, \ldots, 9$ (solid curves). Dashed curves show the leading-order asymptotic values of R_{cr} for $\gamma_2 \gg 1$.

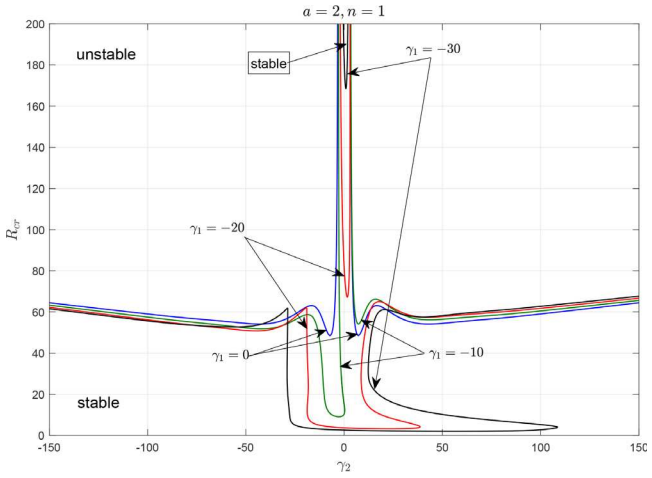

FIG. 17. Converging flow with the pressure-no-slip conditions: critical R vs γ_2 for $a = 2$, $n = 1$, and $\gamma_1 = 0, -10, -20, -30$.

that for $\gamma_2 = 0$. This explains our earlier observation that the critical curves for all values of γ_2 approach the axis $R = 0$ as $\gamma_1 \to \infty$.

The fact that the flow becomes unstable at an arbitrarily small radial Reynolds number provided that $|\gamma_1|$ is sufficiently large is quite unexpected because (in contrast with the case of the pressure–stress conditions) the basic flow is exactly the same as the one studied in Ref. 13. The only difference is that here the normal velocity condition at the outlet is replaced by the normal stress condition. Thus, we can conclude that the normal stress condition drastically destabilizes the same viscous flow. Note also that Figs. 11(a) and 12(a) show that the destabilizing effect does not weaken if a is increased and remains as strong for $a = 8$ as it is for $a = 2$. This is very different from the pressure–stress conditions, where the destabilizing effect becomes much weaker for $a = 8$.

The asymptotic analysis of Appendix B has an interesting by-product, namely, it turns out that the Couette flow between rotating cylinders (with a rotating impermeable inner cylinder and a non-rotating permeable outer cylinder) is linearly unstable to two dimensional perturbations provided that the pressure-no-slip conditions are imposed at the outer cylinder. This is in contrast with the well-known fact that the classical Couette flow (with the normal velocity condition at the outer cylinder) is stable to two-dimensional perturbations.

2. Converging flow

Figure 15 shows neutral curves for the converging flows with the pressure-no-slip conditions for $\gamma_1 = 0$ and $a = 2$. The curves in the top half of the picture for $n = 1, \ldots, 5$ are very similar to the neutral curves in the reference problem. These curves are associated with the inviscid instability described in Sec. III. They approach the vertical asymptotes $\gamma_2 = \gamma_2^*(a, n)$, where $\gamma_2^*(a, n)$ is the inviscid instability boundary on the (a, γ_2) plane, shown in Fig. 3. For each azimuthal mode with $n = 4, \ldots, 7$, there are another two disjoint regions where the corresponding modes are unstable. This is also true for the mode with $n = 3$ but only one of the two regions is visible, as the other is outside the range of γ_2 in Fig. 15. For higher n, these two regions merge into a single one (e.g., the curves for $n = 8$ and 9).

The instability regions that are in the right half of the figure, but not too close to the horizontal axis $R = 0$ are qualitatively similar to those discussed in Ref. 13 and associated with the instability of the boundary layer at the outlet (which reduces to the instability of the asymptotic suction profile for $R \gg 1$). The instability regions that lie near the horizontal axis represent a new instability. Figure 16 shows that the lower boundary of these approaches is $R = 0$ as $\gamma_2 \to \infty$. Asymptotic behavior of these curves for $\gamma_2 \gg 1$ can be analyzed in exactly the same manner as it was done for the diverging flows. It is shown in Appendix B that, in leading order, the critical values of R are given by

$$R_{cr} = \frac{Re_{2cr}(a, n)}{\gamma_2} + O\left(\gamma_2^{-2}\right), \tag{50}$$

where $Re_{2cr}(a, n)$ is a critical value of the second azimuthal Reynolds number, Re_2, defined by Eq. (19). The leading-order approximations given by Eq. (50) and the critical curves obtained by solving the original eigenvalue problem are shown as dashed and solid curves, respectively, in Fig. 16. Evidently, the dashed curves approach the solid curves as γ_2 increases, confirming that the asymptotic formula (50) is correct. Again, a by-product of the asymptotic analysis is that the classical Couette flow with a rotating impermeable outer cylinder and a non-rotating permeable inner cylinder is unstable to two-dimensional perturbations if the pressure-no-slip conditions are imposed at the inner cylinder. This is even more surprising than the analogous result for the diverging flow because it is well known that the classical Couette flow is stable even to three-dimensional perturbations when the inner cylinder is not rotating (see, e.g., Refs. 35 and 36).

Figure 17 shows critical curves for $a = 2$, $n = 1$ and $\gamma_1 = 0, -10, -20$, and -30. Critical curves for the same a and n and for $\gamma_1 = 0, 10, 20$, and 30 can be obtained by reflecting the curves in Fig. 17 about the vertical axis $\gamma_2 = 0$. For very high R ($R \to \infty$), all critical curves approach the same vertical asymptotes as before for all values of γ_1. It is interesting to note that the curves for $\gamma_1 = -10, -20$, and -30 cross the vertical axis $\gamma_2 = 0$. For sufficiently large $|\gamma_1|$, there is a finite interval in R where the flow is unstable even for $\gamma_2 = 0$. For $\gamma_1 = \pm 10$, the flow is unstable if $R \in (10.38, 14.904)$; for $\gamma_1 = \pm 20$, if $R \in (3.693, 81.635)$; for $\gamma_1 = \pm 30$, if $R \in (2.588, 182.578)$. Such behavior of neutral curves means that the basic flow may be unstable even if the azimuthal velocity at the inlet is zero, which is in contrast with the case of the reference condition where it had not been observed. We note in passing that a similar result is also valid in the case of the pressure-stress conditions for basic flows with nonzero s_0.

V. DISCUSSION

The results presented above describe the possible effects of boundary conditions on permeable boundaries on the stability of viscous incompressible flows, driven by these boundary conditions. We have compared the stability properties of three families of steady flows between permeable cylinders, which satisfy the same boundary conditions at the inlet, but different conditions at the outlet, taking the boundary conditions that prescribe the full velocity vector on both cylinders as a reference point. For the other two families, the boundary conditions prescribe all components of the velocity at the inlet and the normal stress and either tangential stress or tangential velocity at the outlet.

In the limit of high radial Reynolds numbers, all three families tend to a single inviscid flow. This inviscid flow satisfies the same inflow boundary conditions, but the outflow conditions reduce to a single condition prescribing either the pressure or the normal velocity. The inviscid flow becomes unstable if the azimuthal velocity at the inlet is greater than a certain critical value. For a weak radial flow, this inviscid instability has the same mechanism for both inviscid outflow conditions, but, overall, the flows with the pressure condition are more unstable than those with the normal velocity condition.

As one would expect, all three families of viscous flows are unstable due to the inviscid instability mechanism for sufficiently high R. However, it turned out that, for moderate and small radial Reynolds numbers, a change in the type of the outflow conditions can drastically change the stability properties of the flow. In most cases, the pressure-stress and pressure-no-slip conditions have a strong destabilizing effect, because these conditions are less restrictive than the reference conditions. (They allow perturbations with the nonzero radial velocity at the outlet.) In particular, in the problem with the pressure-no-slip conditions, both the diverging and converging flows turned out to be unstable for arbitrarily small R, provided that the azimuthal velocity at the inlet is much higher than the radial velocity. In these cases, we have derived asymptotic formulas for critical radial Reynolds numbers, which agree with numerical calculations.

As a by-product of these asymptotic formulas, we have found that two particular cases of the classical Couette flow, where the impermeable cylinder is rotating and the permeable cylinder is stationary, are unstable to two-dimensional perturbations provided that the normal stress condition (instead of the normal velocity condition) at the permeable cylinder is imposed. This is in contrast with the well-known fact that the Couette flow is stable to two-dimensional perturbations. Moreover, in the case where the inner cylinder is non-rotating, the classical Couette flow is stable even to three-dimensional perturbations (e.g., Refs. 35 and 36). The reason for this instability is that the normal stress condition at a permeable wall allows nonzero flow through this wall. Typical contour plots of the stream function of neutral perturbations for both cases of the Couette flow are shown in Fig. 18. Evidently, for these neutral modes, the normal velocity at the permeable cylinder is nonzero. This is impossible in the case of the reference boundary conditions.

Another interesting result is that in the case of the pressure-no-slip condition, there are flow regimes where the converging flows are unstable even if the azimuthal velocity at the inlet is zero as one can see in Fig. 17. In contrast with this observation, the reference conditions do not allow even three-dimensional unstable modes.

The main conclusion of this paper is that boundary conditions at the outlet, which includes the normal stress condition may completely change the stability of the flow. This is particularly apparent in the case of the pressure-no-slip conditions where the basic steady flow is exactly the same as the one considered in Ref. 13.

It is known[13] that, in addition to an inviscid instability, there is another instability in the problem with the reference boundary conditions and that it is related to the instability of the boundary layer at the outlet. For problems considered here, we have not found such instability in the case of pressure–stress conditions. However, for the converging flows with the pressure-no-slip conditions, for some azimuthal modes (with $n = 3, \ldots, 7$), there are three different instability domains (see Fig. 15) where instability has different mechanisms: inviscid instability, instability of the boundary layer at the outlet, and instability due to the instability of the classical Couette flow discussed above. For the diverging flows with the pressure-no-slip conditions, Figs. 11 and 12 show that the instability domain already covers almost the entire (γ_1, R) plane. Even if there were different mechanisms of instability in different regions of the plane, it would be impossible to identify those regions.

There are many open questions in this area. Here, we mention only two, perhaps, the most important questions. The first one concerns three-dimensional perturbations. As we have shown, for the diverging flows for $a = 2$, the most unstable inviscid perturbation is two-dimensional and we expect this to be also true for the converging flows and for different values of a. This implies that at least for sufficiently high radial Reynolds numbers, the most unstable perturbations are very likely to be two-dimensional (as it occurs in the reference problem[15]). Interestingly, even for the classical Couette flow, there are linearly stable flow regimes where the optimal transient growth is achieved on two-dimensional non-modal perturbations.[37] Nonetheless, to obtain a full picture of the instabilities of the flows considered in the present paper, it is necessary to investigate the stability to three-dimensional perturbations.

The second open problem is related to the boundary conditions. As was argued in Sec. II B, the pressure-no-slip conditions may be relevant

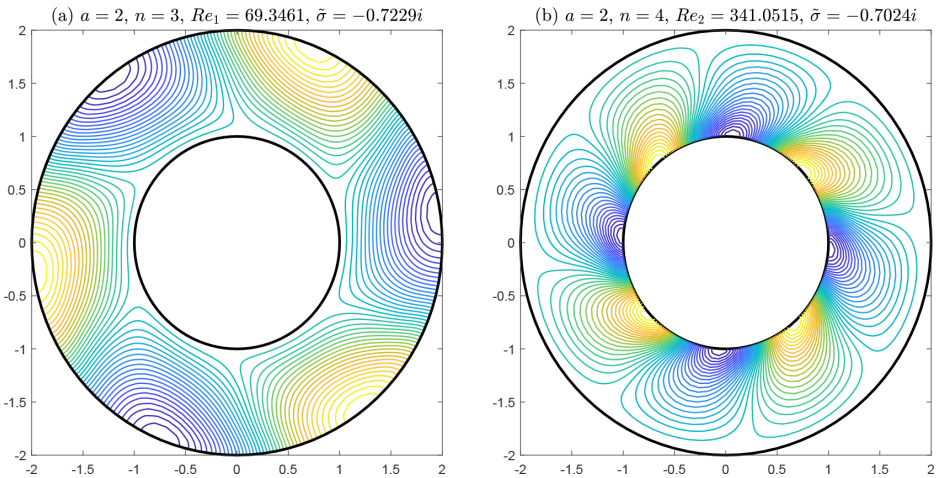

FIG. 18. Neutral modes for the Couette flow between a rotating impermeable cylinder and a stationary permeable cylinder: (a) the outer cylinder is permeable and (b) the inner cylinder is permeable.

to flows between porous cylinders, provided that the pressure in the porous cylinders is known. A better approach would be to consider flows in the free flow domain and in the porous cylinders and match them at the porous walls. An interesting model of this type has been considered in Ref. 38, where flows between a porous cylindrical membrane and an impermeable cylinder were studied, with boundary conditions, obtained using Darcy's law for the flow in the membrane. An asymptotic expression for a steady flow, which includes the axial flow in the gap, in the limit of weak permeability of the membrane has been derived in Ref. 38, and its stability has been studied in Ref. 39. It is worth discussing briefly the connection of the normal stress condition with the condition of Refs. 38 and 39. The boundary condition used in those papers is $u|_{r=1} = -\varkappa(p|_{r=1} - p_0)$, where u and p are the radial velocity and the pressure of the free fluid at the porous membrane (the inner cylinder), p_0 is the pressure on the other side of the membrane, and $\varkappa$ is the non-dimensional permeability of the membrane. Tilton *et al.*[38] studied the case of small permeability $\varkappa \ll 1$. In the opposite case, when $\varkappa \gg 1$, the above condition reduces to $p|_{r=1} = p_0$, and this is almost the same as the normal stress condition $-p|_{r=1} + (2/R)\, u_r|_{r=1} = -p_0$, except for one additional term. Although the above papers make an important contribution to this area of research, the effect of the boundary conditions employed in these papers on the stability of steady flows without axial flow has not been studied there and remains an open problem, and this is a subject of a continuing investigation.

ACKNOWLEDGMENTS

The authors want to thank Professor V. A. Vladimirov for helpful discussions. A. Morgulis would like to acknowledge the continuing support of the Southern Federal University (Rostov-on-Don).

AUTHOR DECLARATIONS

Conflict of Interest

The authors have no conflicts to disclose.

Author Contributions

Konstantin Ilin: Investigation (equal); Methodology (equal); Writing – original draft (equal); Writing – review and editing (equal). **Andrey Morgulis:** Investigation (equal); Methodology (equal); Writing – review and editing (equal).

DATA AVAILABILITY

The data that support the findings of this study are available within the article.

APPENDIX A: ASYMPTOTIC STABILITY TO PERTURBATIONS INDEPENDENT OF Θ

Here, we show that the basic steady flows (12)–(14) are asymptotically stable to two-dimensional axisymmetric perturbations of arbitrary amplitude. In particular, this means that if $n = 0$, then $\mathrm{Re}(\sigma) < 0$, i.e., the mode with $n = 0$ cannot be unstable.

Let

$$u = \frac{\beta}{r} + \tilde{u}(r,t), \quad v = V_\beta(r) + \tilde{v}(r,t),$$

where $V_\beta(r)$ is given by (12), and $\tilde{u}(r,t)$ and $\tilde{v}(r,t)$ represent an axisymmetric perturbation of finite amplitude. Substituting these into Eq. (20), we obtain

$$\left(\partial_t + \frac{\beta}{r}\,\partial_r\right)\tilde{u} - \frac{\beta}{r^2}\,\tilde{u} - \frac{2V_\beta}{r}\,\tilde{v} + \tilde{u}\tilde{u}_r - \frac{\tilde{v}^2}{r} = -\tilde{p}_r + \frac{1}{R}\left(L_0\tilde{u} - \frac{\tilde{u}}{r^2}\right),$$
$$\left(\partial_t + \frac{\beta}{r}\,\partial_r\right)\tilde{v} + \frac{\beta}{r^2}\,\tilde{v} + \Omega_\beta\tilde{u} + \tilde{u}\tilde{v}_r + \frac{\tilde{u}\tilde{v}}{r} = \frac{1}{R}\left(L_0\tilde{v} - \frac{\tilde{v}}{r^2}\right),$$
$$(r\tilde{u})_r = 0.$$

Here, $\tilde{p}$ is the perturbation pressure and $L_0 = \partial_r^2 + r^{-1}\partial_r$. The boundary conditions for $\tilde{u}$ at the inlet are $\tilde{u}|_{r=1} = 0$ for the diverging flow ($\beta = 1$) and $\tilde{u}\,|_{r=a} = 0$ for the converging flow ($\beta = -1$). The incompressibility condition, together with these boundary conditions, implies that $\tilde{u} \equiv 0$, so that the first two of the above equations simplify to

$$-\frac{2V_\beta}{r}\,\tilde{v} - \frac{\tilde{v}^2}{r} = -\tilde{p}_r,$$
$$\left(\partial_t + \frac{\beta}{r}\,\partial_r\right)\tilde{v} + \frac{\beta}{r^2}\,\tilde{v} = \frac{1}{R}\left(L_0\tilde{v} - \frac{\tilde{v}}{r^2}\right). \tag{A1}$$

The second of these is independent from the first one and should be solved subject to appropriate boundary conditions for $\tilde{v}$, while the first equation can be used to find pressure $\tilde{p}$.

In the case of the pressure-no-slip conditions, we have

$$\tilde{v}|_{r=1} = 0, \quad \tilde{v}|_{r=a} = 0.$$

It had been shown in Ref. 13 that Eq. (A1) with these boundary conditions has only decaying (with time) solutions. This implies asymptotic stability.

Consider now the diverging flow ($\beta = 1$) with the pressure–-stress conditions, i.e.,

$$\tilde{v}(1,t) = 0, \quad \tilde{v}(a,t) - \frac{\tilde{v}(a,t)}{a} = 0. \tag{A2}$$

Let

$$E = \int_1^a \frac{\tilde{v}^2}{2}\, r dr.$$

The equation of the balance of the perturbation energy, E, can be written as

$$\dot{E} + \frac{\tilde{v}^2}{2}\bigg|_{r=a} + \int_1^a \frac{\tilde{v}^2}{r}\, dr = -\frac{1}{R}\int_1^a \left(\tilde{v}_r - \frac{\tilde{v}}{r}\right)^2 r dr. \tag{A3}$$

Equation (A3) follows from the following chain of equalities:

$$\int_1^a \left(\tilde{v}_r - \frac{\tilde{v}}{r}\right)^2 r dr = -\tilde{v}^2|_{r=a} + \int_1^a \left(\tilde{v}_r^2 + \frac{\tilde{v}^2}{r^2}\right) r dr$$
$$= -\int_1^a \left(\tilde{v}_{rr} + \frac{\tilde{v}_r}{r} - \frac{\tilde{v}}{r^2}\right)\tilde{v}\, r dr.$$

[Here, we used integration by parts and boundary conditions (A2).]

For the converging flow ($\beta = -1$), the energy balance does not work so well, and we employ the perturbation angular momentum,

$\Gamma = r\tilde{v}$. In terms of Γ, Eq. (A1) (with $\beta = -1$) takes the following form:

$$\left(\partial_t - \frac{1}{r}\,\partial_r\right)\Gamma = \frac{1}{R}\,r\left(\frac{1}{r}\,\Gamma_r\right)_r. \tag{A4}$$

The boundary conditions for $\Gamma(r,t)$ that follow from (5) and (9) can be written as

$$\Gamma(a,t) = 0, \quad \Gamma_r(1,t) - 2\Gamma(1,t) = 0. \tag{A5}$$

Let

$$M = \int_1^a \frac{\tilde{\Gamma}^2}{2}\,rdr.$$

After multiplying Eq. (A4) by $r\,\Gamma$, integrating it from 1 to a in r and performing standard calculations involving integration by parts, we find that

$$\dot{M} = -\frac{1}{R}\int_1^a \Gamma_r^2\,rdr - \left(1 + \frac{2}{R}\right)\frac{\Gamma^2(1,t)}{2}. \tag{A6}$$

It can be shown that Eqs. (A3) and (A6) imply the inequalities

$$\frac{\dot{E}}{E} \le -C^+(a) \quad \text{and} \quad \frac{\dot{M}}{M} \le -\frac{1}{R}\,C^-(a),$$

where $C^{\pm}$ are positive constants that depend on a only. These estimates yield at least exponential decay of all perturbations.

APPENDIX B: ASYMPTOTIC BEHAVIOR OF NEUTRAL CURVES IN THE LIMITS $\gamma_1 \to \infty$ AND $\gamma_2 \to \infty$

1. Diverging flow

Consider the eigenvalue problem, given by Eqs. (27), (28), (35), and (36), in the limit $\gamma_1 \to \infty$. It follows from Eqs. (12) and (17) with $\beta = 1$ that

$$V(r) = \gamma_1 V_0(r), \quad V_0(r) = -\frac{r^{R+2}}{a^{R+2}-1} + \frac{a^{R+1}}{a^{R+2}-1}\,\frac{1}{r} + O\left(\gamma_1^{-1}\right). \tag{B1}$$

Let

$$\sigma = \gamma_1\tilde{\sigma}. \tag{B2}$$

Substitution of (B1) and (B2) into Eq. (27) yields

$$\left(\tilde{\sigma} + \frac{inV_0}{r}\right)L\hat{\psi} - \frac{in}{r}\,\Omega_0'(r)\hat{\psi} = \frac{1}{Re_1}\,L^2\hat{\psi} + O\left(\gamma_1^{-1}\right), \tag{B3}$$

where Re_1 is the azimuthal Reynolds number defined by Eq. (18).

Now, we make our key assumption that is consistent with the behavior of critical curves in Figs. 11–13, namely, $Re_1 = O(1)$ as $\gamma_1 \to \infty$. With this assumption, the above formula for $V_0(r)$ simplifies to

$$V_0(r) = \frac{1}{a^2-1}\left[\frac{a^2}{r} - r\right] + O\left(\gamma_1^{-1}\right). \tag{B4}$$

Note that if we discard the $O(\gamma_1^{-1})$ term in (B4), then $V_0(r)$ is the same as the azimuthal velocity profile of the classical Couette flow between rotating impermeable cylinders with radii 1 and a in a particular case where the outer cylinder does not rotate, and the inner cylinder rotates with an angular velocity equal to 1.

On substituting (B4) into Eq. (B3), we find that, in the leading order,

$$\left(\tilde{\sigma} + \frac{in}{a^2-1}\left[\frac{a^2}{r^2} - 1\right]\right)L\hat{\psi} = \frac{1}{Re_1}\,L^2\hat{\psi}. \tag{B5}$$

In the leading order, boundary conditions (28), (35), and (36) take the following form:

$$\hat{\psi}(1) = 0, \quad \hat{\psi}'(1) = 0, \quad \hat{\psi}'(a) = 0, \tag{B6}$$

$$\frac{1}{Re_1}\left(\hat{\psi}'''(a) + \frac{1}{a}\,\hat{\psi}''(a) + \frac{4n^2}{a^3}\,\hat{\psi}(a)\right) - \frac{2in}{a(a^2-1)}\,\hat{\psi}(a) = 0. \tag{B7}$$

Thus, we have obtained the eigenvalue problem for $\tilde{\sigma}$. It was solved numerically using the same method as the original eigenvalue problem. We found that each azimuthal mode becomes unstable for Re_1 greater than some critical value Re_{1cr}. The critical azimuthal Reynolds numbers for $a = 2$, 8 and $n = 1, \ldots, 5$ are shown in Table II. Using these and formula (49), we plotted the asymptotic R_{cr} as a function of γ_1 in Fig. 14 (dashed curves).

Now, let us discuss the connection of this result with the classical Couette flow. Evidently, if boundary condition (B7) were replaced by the condition $\hat{\psi}(a) = 0$ (i.e., no normal flow at $r = a$), this eigenvalue problem would coincide with the one arising in the particular case of the classical Couette flow mentioned above. It is known that the Couette flow is linearly stable to two-dimensional perturbations, although there seems to be no formal proof of this fact (see, e.g., Ref. 40). However, with boundary condition (B7), the same flow can be unstable. Recalling that the physical meaning of condition (B7) is that the normal stress applied to the fluid at $r = a$ is zero, we conclude that the Couette flow with the normal stress condition at the outer cylinder (instead of the normal velocity condition) is unstable to two-dimensional perturbations provided that

$$Re_1 > \min_{n\in\mathbb{N}} Re_{1cr}(a,n).$$

TABLE II. $Re_{1cr}(a,n)$.

	$a=2$					$a=8$				
n	1	2	3	4	5	1	2	3	4	5
Re_{1cr}	147.29	77.58	69.35	117.36	188.80	12.54	51.79	100.48	165.39	246.62

TABLE III. $Re_{2cr}(a, n)$ for $a = 2$.

n	4	5	6	7	8	9
Re_{2cr}	341.05	546.34	793.46	1093.4	1444.3	1845.7

2. Converging flow

Consider the eigenvalue problem, given by Eqs. (27), (29), (35), and (37), in the limit $\gamma_2 \to \infty$. The same arguments as for the diverging flow yield, in the leading order, the following eigenvalue problem for $\tilde{\sigma} = \sigma/\gamma_2$:

$$\left(\tilde{\sigma} + \frac{in}{a^2-1}\left[1 - \frac{1}{r^2}\right]\right) L\hat{\psi} = \frac{1}{Re_2} L^2\hat{\psi}, \tag{B8}$$

$$\hat{\psi}(a) = 0, \quad \hat{\psi}'(a) = 0, \quad \hat{\psi}'(1) = 0, \tag{B9}$$

$$\frac{1}{Re_2}\left(\hat{\psi}'''(1) + \hat{\psi}''(1) + 4n^2\hat{\psi}(1)\right) + \frac{2in}{a^2-1}\hat{\psi}(1) = 0, \tag{B10}$$

where Re_2 is defined by Eq. (19). Solving this problem numerically, we find that azimuthal modes with $n = 4, \ldots, 9$ become unstable for Re_2 greater than some critical value Re_{2cr}. The critical azimuthal Reynolds numbers for $a = 2$ and $n = 4, \ldots, 9$ are shown in Table III.

REFERENCES

[1] S. K. Bahl, "Stability of viscous flow between two concentric rotating porous cylinders," Def. Sci. J. **20**(2), 89 (1970), available at https://publications.drdo.gov.in/ojs/index.php/dsj/article/view/6132.

[2] K. Min and R. M. Lueptow, "Hydrodynamic stability of viscous flow between rotating porous cylinders with radial flow," Phys. Fluids **6**(1), 144 (1994).

[3] E. C. Johnson and R. M. Lueptow, "Hydrodynamic stability of flow between rotating porous cylinders with radial and axial flow," Phys. Fluids **9**(12), 3687 (1997).

[4] A. A. Kolyshkin and R. Vaillancourt, "Convective instability boundary of Couette flow between rotating porous cylinders with axial and radial flows," Phys. Fluids **9**, 910 (1997).

[5] V. Kolesov and L. Shapakidze, "On oscillatory modes in viscous incompressible liquid flows between two counter-rotating permeable cylinders," in *Trends in Applications of Mathematics to Mechanics*, edited by O. G. G. Iooss and A. Nouri (Chapman and Hall/CRC, 1999), pp. 221–227.

[6] E. Serre, M. A. Sprague, and R. M. Lueptow, "Stability of Taylor–Couette flow in a finite-length cavity with radial throughflow," Phys. Fluids **20**(3), 034106 (2008).

[7] D. Martinand, E. Serre, and R. M. Lueptow, "Absolute and convective instability of cylindrical Couette flow with axial and radial flows," Phys. Fluids **21**(10), 104102 (2009).

[8] B. Gallet, C. R. Doering, and E. A. Spiegel, "Destabilizing Taylor–Couette flow with suction," Phys. Fluids **22**(3), 034105 (2010).

[9] H. Fujita, H. Morimoto, and H. Okamoto, "Stability analysis of Navier–Stokes flows in annuli," Math. Methods Appl. Sci. **20**(11), 959 (1997).

[10] R. R. Kerswell, "Instability driven by boundary inflow across shear: A way to circumvent Rayleigh's stability criterion in accretion disks?," J. Fluid Mech. **784**, 619 (2015).

[11] D. Martinand, E. Serre, and R. M. Lueptow, "Linear and weakly nonlinear analyses of cylindrical Couette flow with axial and radial flows," J. Fluid Mech. **824**, 438 (2017).

[12] K. Ilin and A. Morgulis, "Instability of an inviscid flow between porous cylinders with radial flow," J. Fluid Mech. **730**, 364 (2013).

[13] K. Ilin and A. Morgulis, "Instability of a two-dimensional viscous flow in an annulus with permeable walls to two-dimensional perturbations," Phys. Fluids **27**, 044107 (2015).

[14] K. Ilin and A. Morgulis, "Inviscid instability of an incompressible flow between rotating porous cylinders to three-dimensional perturbations," Eur. J. Mech.—B/Fluids **61**(1), 46 (2017).

[15] K. Ilin and A. Morgulis, "On the stability of the Couette–Taylor flow between rotating porous cylinders with radial flow," Eur. J. Mech.—B/Fluids **80**(1), 174 (2020).

[16] S. Wroński, E. Molga, and L. Rudniak, "Dynamic filtration in biotechnology," Bioprocess Eng. **4**(3), 99 (1989).

[17] G. Beadoin and M. Y. Jaffrin, "Plasma filtration in Couette flow membrane devices," Artif. Organs **13**(1), 43 (1989).

[18] R. C. Giordano, R. L. C. Giordano, D. M. F. Prazerest, and C. L. Cooney, "Analysis of a Taylor–Poiseuille vortex flow reactor—I: Flow patterns and mass transfer characteristics," Chem. Eng. Sci. **53**(20), 3635 (1998).

[19] E. Kersale, D. W. Hughes, G. I. Ogilvie, S. M. Tobias, and N. O. Weiss, "Global magnetorotational instability with inflow. I. Linear theory and the role of boundary conditions," Astrophys. J **602**(2), 892 (2004).

[20] Y. Tsujimoto, Y. Yoshida, and Y. Mori, "Study of vaneless diffuser rotating stall based on two-dimensional inviscid flow analysis," ASME J. Fluids Eng. **118**, 123 (1996).

[21] S. S. Ljevar, H. C. de Lange, and A. A. van Steenhoven, "Comparison of a two-dimensional viscid and inviscid model for rotating stall analysis," in *Proceedings of the 4th WSEAS International Conference on Fluid Mechanics and Aerodynamics, Elounda, Greece, August 21–23, 2006* (WSEAS, 2006), pp. 376–383.

[22] S. Guadagni, M. Giachi, L. Fusi, and A. Farina, "Flow stability in a wide vaneless diffuser," Appl. Eng. Sci. **4**, 100025 (2020).

[23] F. Gallaire and J.-M. Chomaz, "The role of boundary conditions in a simple model of incipient vortex breakdown," Phys. Fluids **16**(2), 274–286 (2004).

[24] P. M. Gresho, "Incompressible fluid dynamics: Some fundamental formulation issues," Ann. Rev. Fluid Mech. **23**, 413 (1991).

[25] M. D. Gunzburger, *Finite Element Methods for Viscous Incompressible Flows: A Guide to Theory, Practice, and Algorithms* (Academic Press, Boston, 1989).

[26] G. S. Beavers and D. D. Joseph, "Boundary conditions at a naturally permeable wall," J. Fluid Mech. **30**, 197 (1967).

[27] P. G. Saffman, "On the boundary condition at the surface of a porous medium," Stud. Appl. Math. **50**(2), 93 (1971).

[28] S. Haber and R. Mauri, "Boundary conditions for Darcy's flow through porous media," Int. J. Multiphase Flow **9**(5), 561 (1983).

[29] J. T. Ault, B. Rallabandi, O. Shardt, K. K. Chen, and H. A. Stone, "Entry and exit flows in curved pipes," J. Fluid Mech. **815**, 570 (2017).

[30] V. Citro, L. Siconolfi, D. Fabre, F. Giannetti, and P. Luchini, "Stability and sensitivity analysis of the secondary instability in the sphere wake," AIAA J. **55**(11), 3661 (2017).

[31] D. Sipp and A. Lebedev, "Global stability of base and mean flows: A general approach and its applications to cylinder and open cavity flows," J. Fluid Mech. **593**, 333 (2007).

[32] M. Bukač, S. Čanić, R. Glowinski, J. Tambača, and A. Quaini, "Fluid–structure interaction in blood flow capturing non-zero longitudinal structure displacement," J. Comput. Phys. **235**, 515 (2013).

[33] M. Bukač, S. Čanić, J. Tambača, and Y. Wang, "Fluid–structure interaction between pulsatile blood flow and a curved stented coronary artery on a beating heart: A four stent computational study," Comput. Methods Appl. Mech. Eng. **350**, 679 (2019).

[34] D. Gottlieb and S. A. Orszag, *Numerical Analysis of Spectral Methods: Theory and Applications*, CBMS-NSF Regional Conference Series in Applied Mathematics (SIAM, Philadelphia, 1977).

[35] C. D. Andereck, S. S. Liu, and H. L. Swinney, "Flow regimes in a circular Couette system with independently rotating cylinders," J. Fluid Mech. **164**, 155 (1986).

[36] P. Chossat and G. Iooss, *The Couette–Taylor Problem*, Applied Mathematical Sciences Vol. 102 (Springer, New York, 1994).

[37] S. Maretzke, B. Hof, and M. Avila, "Transient growth in linearly stable Taylor–Couette flows," J. Fluid Mech. **742**, 254 (2014).

[38] N. Tilton, D. Martinand, E. Serre, and R. M. Lueptow, "Pressure-driven radial flow in a Taylor–Couette cell," J. Fluid Mech. **660**, 527 (2010).

[39] N. Tilton and D. Martinand, "Taylor–Couette–Poiseuille flow with a weakly permeable inner cylinder: Absolute instabilities and selection of global modes," J. Fluid Mech. **849**, 741 (2018).

[40] P. G. Drazin and W. H. Reid, *Hydrodynamic Stability* (Cambridge University Press, 1981).